Acta Mech 229, 719–743 (2018)
https://doi.org/10.1007/s00707-017-1995-0

ORIGINAL PAPER

Qiushi Fu · Jiang Qian · Dimitri E. Beskos

Inelastic anisotropic constitutive models based on evolutionary linear transformations on stress tensors with application to masonry

This paper is dedicated to the memory of Franz Ziegler

Received: 3 March 2017 / Revised: 14 May 2017 / Published online: 17 November 2017

Abstract The formulation of constitutive models for anisotropic materials such as masonry is a problem of large complexity. One possible way is to define linear transformations on the stress tensors using fourth-order transformation tensors that carry all the anisotropic information of the material. In the present paper, a new type of evolutionary linear transformation tensor is defined, which can change the values of its components along with the evolution of internal variables. This means the transformation laws are defined according to the current plastic and damage levels, and allows the constitutive model to describe totally different hardening and softening behaviours of the material along different directions. First, a general procedure of formulation of anisotropic constitutive models is given. Second, as a specific example, an orthotropic plastic–damage constitutive model for masonry is presented. Finally, the proposed constitutive model is validated by comparing finite element results with experimental ones pertaining to simple masonry structures under static and cyclic loading.

1 Introduction

Masonry is the oldest building material that still finds wide use in todays building construction. In many countries, the existing building heritage mainly consists of masonry structures, including monuments of enormous architectural and historical value. The study of the behaviour of masonry structures is still of great importance [1]. Owing to the particular geometric arrangement of units (bricks, blocks) and mortar joints, masonry exhibits macroscopically an overall orthotropic behaviour. In general, masonry structures can be analysed by employing micro-modelling and macro-modelling procedures [2,3].

Micro-modelling, including both detailed micro-modelling and simplified micro-modelling, is considered the most accurate tool available to analyse masonry, since the discretization is carried down to the level of the constituents. In detailed micro-models, the units and the mortar at joints are described with continuum

Q. Fu · J. Qian · D. E. Beskos (✉)
Institute of Structural Engineering and Disaster Reduction, College of Civil Engineering, Tongji University, Shanghai 200092, China
E-mail: dimisof@hotmail.com

Q. Fu
E-mail: qiushi.fu@gmail.com

J. Qian
State Key Laboratory of Disaster Reduction in Civil Engineering, College of Civil Engineering, Tongji University, Shanghai 200092, China
E-mail: jqian@mail.tongji.edu.cn

D. E. Beskos
Department of Civil Engineering, University of Patras, 26500 Patras, Greece

finite elements, and the unit-mortar interface is represented by discontinuous elements accounting for potential crack or slip planes [4]. The detailed micro-modelling strategy leads to very accurate results, but requires large computational effort. The simplified micro-modelling strategy can, to some extent, overcome this drawback. In this strategy, expanded units represented by continuum elements are used to model both units and mortar material, while the behaviour of the mortar joints and unit-mortar interfaces is lumped to the discontinuous elements [5–10]. Still, applicability of both strategies of micro-modelling is generally limited to structural details because of the intensive computational effort.

Macro-modelling, to some extent, is a compromise between accuracy and efficiency. In large-scale, especially practice-oriented analyses, detailed descriptions of interactions between units and mortar may not be necessary. On these occasions, macro-modelling strategies, although not making any distinction between units and joints, may still give satisfactory estimations of structural responses. Generally, the macro-models are related to plasticity or damage constitutive laws. One can mention here the works of Cervera et al. [11] and Faria et al. [12] on isotropic plastic–damage models and Hatzigcorgiou and Beskos [13,14] on isotropic elastic damage models and their applications in concrete and masonry structures via finite and boundary element methods. At this point the recent theoretical works of Voyiadjis and Kattan [15] and Baratta et al. [16] on elastic damage with applications to masonry solids should be also mentioned. In the works of Lourenço et al. [17,18], orthotropic continuum models were developed based on plasticity theory consisting of a Hill-type yield criterion for compression and a Rankine-type yield criterion for tension. Internal parameters related to both tensile and compressive fracture energies were adopted in order to guarantee mesh objectivity. In the case of damage models, a number of orthotropic models has been also proposed. Berto et al. [19] developed a specific damage model for orthotropic brittle materials with different elastic and inelastic properties along the two material directions. The basic assumption of the model is the acceptance of the natural axes of the masonry (i.e. the bed joints and the head joints directions) also as principal axes of the damage.

Homogenization techniques [20,21] can be seen as a bridge connecting micro-models and macro-models. On the one hand, by using this technique, an anisotropic macro-constitutive law can be obtained from the micro-constitutive laws and geometry of the composite in such a way that the macro-constitutive law is not actually implemented. On the other hand, material data can be obtained by using the homogenization technique as input data for independent macro-models. One quite popular method of homogenization simplifies the geometry of the basic unit with a two-step introduction of vertical and horizontal joints and thus without taking into account the regular offset of vertical mortar joints [4]. However, this method results in significant errors when the difference of stiffness of mortar and units is large, which is a very common situation in nonlinear analyses. A more precise technique called micromechanical homogenization is based on the detailed investigation of the elementary cell and overcomes the approximations introduced by the two-step simplified method [22–24].

Considering the fact that today micro-modelling and homogenization approaches still require considerable computational effort when facing real case studies, the present study still focuses on macro-modelling strategy. The effective constitutive behaviour of masonry features anisotropy arising from the geometrical arrangement of units and mortar, even if the properties of these constituents are isotropic. Therefore, an anisotropic constitutive model is required.

As is well known, the formulation of realistic constitutive models for anisotropic solids is a problem of large complexity. Meanwhile, in inelasticity there exist many well-developed isotropic constitutive models [25]. Therefore, one can obtain anisotropic constitutive models by appropriately extending isotropic ones. This extension can be achieved by a method based on linear transformation on stress or strain tensors.

Linear transformations on stress tensors were first introduced by Sobodka [26], Boehler and Sawczuck [27], and Betten [28]. Barlat et al. [29] applied this method to a full stress state. Karafillis and Boyce [30] considered a linear transformation of the actual stress tensor acting on the anisotropic material. This linear transformation weights the different components of the stress tensor of the anisotropic material in order to account for the anisotropy of the material. Additionally, in the works of Oller et al. [31,32], linear transformations on both stress and strain tensors were defined, although the underlying mathematical concept is still almost equivalent to that in previous studies. This approach was adopted by Pelà et al. [33,34] to the masonry material under the framework of elastic damage mechanics.

It is worth noting that the linear transformation method discussed in the studies mentioned above mainly deals with initial anisotropy rather than evolutionary anisotropy, which means different hardening or softening behaviours along different material directions cannot be fully described. Constitutive models thus developed perform well on conditions where evolutionary anisotropy can be neglected. Thus, there is a need for a development of anisotropic models that can account for both initial and evolutionary anisotropy.

In the present study, an approach named evolutionary linear transformation is proposed, which is based on the existing linear transformation approach. By introducing an evolutionary transformation tensor with changing values of its components according to the levels of material plasticity and damage evolution, a new methodology for extending an isotropic plastic and/or damage constitutive model to an anisotropic one with evolutionary anisotropy is presented and applied to masonry structures.

First, the concept of evolutionary linear transformation is defined, and a kind of evolutionary transformation tensor is proposed. Since these tensors are functions of internal variables, the values of their components can change according to the levels of plasticity and damage evolutions, and therefore enable the constitutive models to describe different mechanical characteristics along different material directions. A general approach of establishing anisotropic constitutive models based on the proposed evolutionary transformation tensor is provided.

Second, the main failure modes of masonry are introduced, and it is pointed out that in macro-models, which make no distinction between units and mortars, it is impossible to describe the Mode II slip failure of bed joints using only the tensile and compressive damage variables. For this reason, the present study proposes an additional damage variable describing the Mode II failure.

Finally, the constitutive model proposed in the paper is used in conjunction with the finite element method to simulate experiments. It is shown that the proposed model is able to successfully reproduce masonry mechanical behaviour under static and cyclic loading.

2 Definition of the evolutionary linear transformation approach

Consider the stress tensor $\boldsymbol{\sigma}$ defined in the real space for an anisotropic inelastic material model and the transformed stress tensor defined in the transformed space for the corresponding isotropic inelastic material model and obtained by the linear transformation

$$\boldsymbol{\sigma}^* = \boldsymbol{A} : \boldsymbol{\sigma} \tag{1}$$

where $\boldsymbol{A}$ denotes the fourth-order transformation tensor which includes the anisotropy effects and weights the different components of the stress tensor $\boldsymbol{\sigma}$ in accordance with the anisotropy of the material. Thus, an anisotropic constitutive model can be simply obtained on the basis of the known constitutive equation of its corresponding isotropic model and the transformation tensor [27,29–31,35,36].

In all previous studies, tensor $\boldsymbol{A}$ was assumed to remain constant during the loading process of the material, which implies that transformation laws for the material under different plastic or damage evolution levels are the same. Anisotropic constitutive models thus developed cannot predict totally independent hardening or softening behaviours along different material directions. In other words, only initial anisotropic behaviours of the material can be considered. In order to develop constitutive models that can also account for evolutionary anisotropy, a new linear transformation approach, named "evolutionary linear transformation," is developed in the present paper. In this approach, the transformation tensor $\boldsymbol{A}$ is no longer fixed. On the contrary, it is a function of k internal variables $\boldsymbol{V}_k$ of the inelastic constitutive law of the material, i.e.

$$\boldsymbol{A} = \boldsymbol{A}\left(\boldsymbol{V}_k\right). \tag{2}$$

This means that the transformation law is defined according to the current plastic and damage levels and allows the constitutive model to describe totally different hardening and softening behaviours of the material along different directions. There are many possible forms that transformation tensor $\boldsymbol{A}$ can take [27,29–31,35,36]. In this Section, no particular form of $\boldsymbol{A}$ is adopted because the goal here is to give a general procedure for the establishment of anisotropic plastic and/or damage constitutive models. However, in Sect. 3, a specific diagonal form of $\boldsymbol{A}$ is adopted for masonry material.

In the following part of this Section, methods for establishing anisotropic constitutive models under elasto-plastic mechanics or damage mechanics are discussed separately. However, these procedures can also be used together to formulate a plastic–damage constitutive model, as illustrated in Sect. 3.

2.1 Formulation of an elastoplastic constitutive model using evolutionary linear transformation

Consider the anisotropic yielding and plastic potential functions F and F^p, respectively, of the form

$$\begin{aligned} F\left(\boldsymbol{\sigma}, \kappa\right) &= 0, \\ F^p\left(\boldsymbol{\sigma}, \kappa\right) &= 0 \end{aligned} \tag{3}$$

where κ is the internal variable that describes the extent of plastic evolution. Since this Subsection currently deals with elastoplastic constitutive models, Eq. (1) becomes

$$\boldsymbol{\sigma}^* = \boldsymbol{A}^{\sigma,p} : \boldsymbol{\sigma} \tag{4}$$

where $\boldsymbol{A}^{\sigma,p}$ is the fourth-order evolutionary transformation tensor. The upper script σ, p indicates that the transformation tensor is used for the transformation of the stress tensor in a plastic constitutive model. The following developments are based on the classical work hardening non-associated theory of plasticity [37]. Functions F^* and F^{p*} are known isotropic yielding and plastic potential functions, respectively, of the form

$$\begin{aligned} F^* \left(\boldsymbol{\sigma}^*, \kappa\right) &= 0, \\ F^{p*} \left(\boldsymbol{\sigma}^*, \kappa\right) &= 0. \end{aligned} \tag{5}$$

It is assumed that the transformation tensor $\boldsymbol{A}^{\sigma,p}$ contains all the information concerning the real anisotropic material. Using Eq. (4) in Eq. (5) one can obtain

$$\begin{aligned} F^* \left(\boldsymbol{\sigma}^*, \kappa\right) &= F^* \left(\boldsymbol{A}^{\sigma,p} : \boldsymbol{\sigma}, \kappa\right) = F\left(\boldsymbol{\sigma}, \kappa\right), \\ F^{p*} \left(\boldsymbol{\sigma}^*, \kappa\right) &= F^* \left(\boldsymbol{A}^{\sigma,p} : \boldsymbol{\sigma}, \kappa\right) = F^p\left(\boldsymbol{\sigma}, \kappa\right). \end{aligned} \tag{6}$$

Differentiating Eq. (6) with respect to $\boldsymbol{\sigma}$ and invoking the chain rule, one has that

$$\frac{\partial F}{\partial \boldsymbol{\sigma}} = \frac{\partial F^*}{\partial \boldsymbol{\sigma}^*} : \frac{\partial \boldsymbol{\sigma}^*}{\partial \boldsymbol{\sigma}} = \frac{\partial F^*}{\partial \boldsymbol{\sigma}^*} : \boldsymbol{A}^{\sigma,p}, \tag{7}$$

$$\frac{\partial F^p}{\partial \boldsymbol{\sigma}} = \frac{\partial F^{p*}}{\partial \boldsymbol{\sigma}^*} : \frac{\partial \boldsymbol{\sigma}^*}{\partial \boldsymbol{\sigma}} = \frac{\partial F^{p*}}{\partial \boldsymbol{\sigma}^*} : \boldsymbol{A}^{\sigma,p}. \tag{8}$$

According to Eq. (8), the flow rule can be expressed as

$$\dot{\boldsymbol{\varepsilon}}^p = \dot{\lambda} \frac{\partial F^p}{\partial \boldsymbol{\sigma}} = \dot{\lambda} \frac{\partial F^{p*}}{\partial \boldsymbol{\sigma}^*} : \frac{\partial \boldsymbol{\sigma}^*}{\partial \boldsymbol{\sigma}} = \dot{\lambda} \frac{\partial F^{p*}}{\partial \boldsymbol{\sigma}^*} : \boldsymbol{A}^{\sigma,p} \tag{9}$$

where $\dot{\boldsymbol{\varepsilon}}^p$ is the plastic strain rate tensor and $\dot{\lambda}$ is the plastic multiplier rate. Furthermore, one has that

$$\begin{aligned} \frac{\partial F}{\partial \kappa} &= \frac{\partial F^*}{\partial \kappa} + \frac{\partial F^*}{\partial \boldsymbol{\sigma}^*} : \frac{\partial \boldsymbol{\sigma}^*}{\partial \kappa} \\ &= \frac{\partial F^*}{\partial \kappa} + \frac{\partial F^*}{\partial \boldsymbol{\sigma}^*} : \frac{\partial \left(\boldsymbol{A}^{\sigma,p} : \boldsymbol{\sigma}\right)}{\partial \kappa} \\ &= \frac{\partial F^*}{\partial \kappa} + \frac{\partial F^*}{\partial \boldsymbol{\sigma}^*} : \frac{\partial \left(\boldsymbol{A}^{\sigma,p}\right)}{\partial \kappa} : \boldsymbol{\sigma}. \end{aligned} \tag{10}$$

The consistency condition can be expressed as

$$\frac{\partial F}{\partial \boldsymbol{\sigma}} : \dot{\boldsymbol{\sigma}} + \frac{\partial F}{\partial \kappa} \dot{\kappa} = 0. \tag{11}$$

The stress–strain equation in rate form on account of Eq. (9) takes the form

$$\dot{\boldsymbol{\sigma}} = \boldsymbol{C}_0 : \left(\dot{\boldsymbol{\varepsilon}} - \dot{\boldsymbol{\varepsilon}}^p\right) = \boldsymbol{C}_0 : \left(\dot{\boldsymbol{\varepsilon}} - \dot{\lambda} \frac{\partial F^p}{\partial \boldsymbol{\sigma}}\right) \tag{12}$$

where $\boldsymbol{C}^0$ is the initial elastic stiffness tensor and use has been made of the relation $\dot{\boldsymbol{\varepsilon}} = \dot{\boldsymbol{\varepsilon}}^e + \dot{\boldsymbol{\varepsilon}}^p$ with $\boldsymbol{\varepsilon}$ and $\boldsymbol{\varepsilon}^e$ being the total and elastic strain tensors, respectively. Substituting Eq. (12) into (11) yields

$$\dot{\lambda} = \frac{\frac{\partial F}{\partial \boldsymbol{\sigma}} : \boldsymbol{C}^0 : \dot{\boldsymbol{\varepsilon}}}{\frac{\partial F}{\partial \boldsymbol{\sigma}} : \boldsymbol{C}^0 : \frac{\partial F^p}{\partial \boldsymbol{\sigma}} - \frac{\partial F}{\partial \kappa} \frac{\mathrm{d}\kappa}{\mathrm{d}\lambda}}. \tag{13}$$

By substituting Eqs. (7), (8), and (10) into (13), one can obtain

$$\dot{\lambda} = \frac{\frac{\partial F^*}{\partial \boldsymbol{\sigma}^*} : \boldsymbol{A}^{\sigma,p} : \boldsymbol{C}^0 : \dot{\boldsymbol{\varepsilon}}}{\frac{\partial F^*}{\partial \boldsymbol{\sigma}^*} : \boldsymbol{A}^{\sigma,p} : \boldsymbol{C}^0 : \frac{\partial F^{p*}}{\partial \boldsymbol{\sigma}^*} : \boldsymbol{A}^{\sigma,p} - \left(\frac{\partial F^*}{\partial \kappa} + \frac{\partial F^*}{\partial \boldsymbol{\sigma}^*} : \frac{\partial (\boldsymbol{A}^{\sigma,p})}{\partial \kappa} : \boldsymbol{\sigma}\right) \frac{d\kappa}{d\lambda}}. \tag{14}$$

Moreover, substituting Eqs. (9) and (14) into (12), the latter equation becomes

$$\dot{\boldsymbol{\sigma}} = \boldsymbol{C}^{ep} : \dot{\boldsymbol{\varepsilon}} \tag{15}$$

where $\boldsymbol{C}^{ep}$ is the elastoplastic tangent stiffness tensor, which can be expressed as

$$\boldsymbol{C}^{ep} = \boldsymbol{C}^{0} - \frac{1}{H^{*}}\left[\boldsymbol{C}^{0} : \left(\frac{\partial F^{p*}}{\partial \boldsymbol{\sigma}^{*}} : \boldsymbol{A}^{\sigma,p}\right)\right] \otimes \left[\boldsymbol{C}^{0} : \left(\frac{\partial F^{*}}{\partial \boldsymbol{\sigma}^{*}} : \boldsymbol{A}^{\sigma,p}\right)\right] \tag{16}$$

with

$$H^{*} = \frac{\partial F^{*}}{\partial \boldsymbol{\sigma}^{*}} : \boldsymbol{A}^{\sigma,p} : \boldsymbol{C}^{0} : \frac{\partial F^{p*}}{\partial \boldsymbol{\sigma}^{*}} : \boldsymbol{A}^{\sigma,p} - \left(\frac{\partial F^{*}}{\partial \kappa} + \frac{\partial F^{*}}{\partial \boldsymbol{\sigma}^{*}} : \frac{\partial \left(\boldsymbol{A}^{\sigma,p}\right)}{\partial \kappa} : \boldsymbol{\sigma}\right) \frac{\mathrm{d}\kappa}{\mathrm{d}\dot{\lambda}}. \tag{17}$$

Equations (14)–(17) clearly indicate that one can obtain the constitutive equation of the anisotropic elastoplastic model in terms of the constitutive parameters of the corresponding isotropic elastoplastic model and the transformation tensor $\boldsymbol{A}$. The evolutionary character of $\boldsymbol{A}$ is manifested in its dependence on κ ($\partial \boldsymbol{A}^{\sigma,p}/\partial \kappa \neq 0$). From Eqs. (7), (8), and (9), it can be seen that the linear transformation does not change the normality condition of the isotropic constitutive model, which suggests that if one wants to obtain an anisotropic constitutive model with a flow rule that satisfies the normality condition, all that needed is to guarantee $F^{*} = F^{p*}$.

2.2 Formulation of a damage constitutive model using evolutionary linear transformation

From the many different forms of damage criteria functions proposed in the literature, in this Section, the damage criterion is expressed as a general function of effective stress tensors that takes no specific form, in order to demonstrate the general procedure of establishing an anisotropic damage constitutive model. This includes the case of a damage energy release rate-based damage criterion, which enjoys a solid thermodynamic foundation, as a special case. Additionally, extension of the proposed method to the case of damage criteria defined by functions of Cauchy stress tensors or strain tensors is also quite straightforward.

According to the definition of linear transformation, one has

$$\bar{\boldsymbol{\sigma}}^{*} = \boldsymbol{A}^{\bar{\sigma},d} : \bar{\boldsymbol{\sigma}} \tag{18}$$

where $\boldsymbol{A}^{\bar{\sigma},d}$ is the fourth-order transformation tensor for the damage constitutive model, and overbars denote effective stresses. The effective stress $\bar{\boldsymbol{\sigma}}$ is associated with the undamaged part of the body and is related with the total stress $\boldsymbol{\sigma}$ by [38]

$$\boldsymbol{\sigma} = (1 - d)\bar{\boldsymbol{\sigma}} \tag{19}$$

where the scalar $0 \leq d \leq 1$ is the damage index or variable that becomes 0 when there is no damage and 1 when there is complete failure. Physically, damage is defined as the surface density of micro-cracks and intersections of micro-voids [38].

It is assumed that $g(\tau, r)$ and $\tau(\bar{\boldsymbol{\sigma}})$ are the anisotropic damage criterion and corresponding equivalent stress that need to be formulated, respectively, while $\tau^{*}(\bar{\boldsymbol{\sigma}}^{*})$ is the known equivalent stress calculated from the transformed effective stress tensor $\bar{\boldsymbol{\sigma}}^{*}$. Then the anisotropic damage criterion can be expressed as

$$g(\tau, r) = \tau(\bar{\boldsymbol{\sigma}}) - r = \tau^{*}\left(\boldsymbol{A}^{\bar{\sigma},d} : \bar{\boldsymbol{\sigma}}\right) - r \leq 0 \tag{20}$$

where variable r is the current damage threshold value which controls the size of the expanding damage surface [39].

Since an anisotropic material may have different hardening and/or softening behaviours, the shape of the damage threshold surface should be able to change along with the evolution of damage as shown in Fig. 1.

Therefore, the evolutionary transformation tensor $\boldsymbol{A}^{\bar{\sigma},d}$ should be a function of the damage variable d or the damage threshold value r. Here, for convenience $\boldsymbol{A}^{\bar{\sigma},d}$ is defined as

$$\boldsymbol{A}^{\bar{\sigma},d} = \boldsymbol{A}^{\bar{\sigma},d}(r). \tag{21}$$

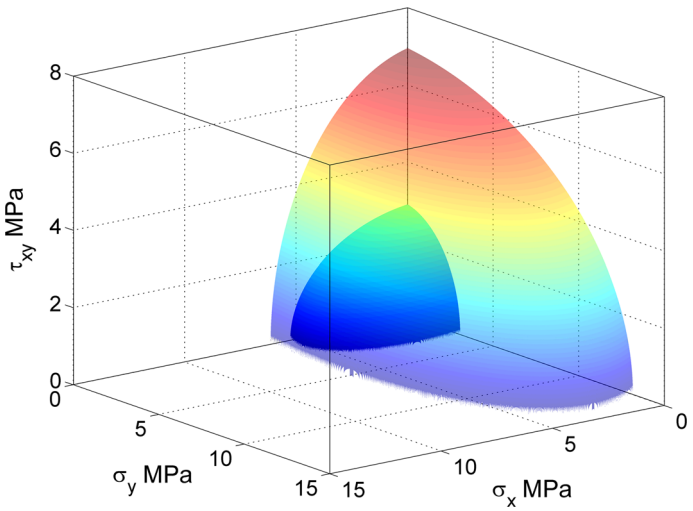

Fig. 1 Shapes of the damage threshold surface at different damage evolution levels. The small surface is the initial damage surface, and the large surface is a subsequent damage surface

According to the consistency condition, during a loading process, one has from Eq. (20) written in rate form

$$\dot{\tau} - \dot{r} = 0\,, \quad \text{or}\,, \quad \mathrm{d}\,\tau - \mathrm{d}\,r = 0, \tag{22}$$

$$\frac{\mathrm{d}\tau}{\mathrm{d}\bar{\boldsymbol{\sigma}}^*}\left(\frac{\partial\left(\boldsymbol{A}^{\bar{\sigma},d}:\bar{\boldsymbol{\sigma}}\right)}{\partial r}\mathrm{d}r + \frac{\partial\bar{\boldsymbol{\sigma}}^*}{\partial\bar{\boldsymbol{\sigma}}}:\mathrm{d}\bar{\boldsymbol{\sigma}}\right) - \mathrm{d}r = 0. \tag{23}$$

Equation (23) is solved for dr and yields

$$\mathrm{d}r = \frac{1}{H^{**}}\frac{\mathrm{d}\tau^*}{\mathrm{d}\bar{\boldsymbol{\sigma}}^*}:\boldsymbol{A}^{\bar{\sigma},d}:\mathrm{d}\bar{\boldsymbol{\sigma}} \tag{24}$$

where

$$H^{**} = 1 - \frac{\mathrm{d}\tau^*}{\mathrm{d}\bar{\boldsymbol{\sigma}}^*}:\frac{\mathrm{d}\boldsymbol{A}^{\bar{\sigma},d}}{\mathrm{d}r}:\bar{\boldsymbol{\sigma}}. \tag{25}$$

The damage variable d can be expressed as

$$d = G\,(r) \tag{26}$$

where $G\,(r)$ is a monotonic function describing the relationship between damage variable d and damage threshold r, which is usually defined according to experimental results. Thus, the rate expression of the stress tensor $\dot{\boldsymbol{\sigma}}$ is of the form

$$\dot{\boldsymbol{\sigma}}\,(\boldsymbol{\varepsilon}, d) = (1-d)\,\boldsymbol{C}^0:\dot{\boldsymbol{\varepsilon}} - \dot{d}\bar{\boldsymbol{\sigma}} = (1-d)\,\boldsymbol{C}^0:\dot{\boldsymbol{\varepsilon}} - \frac{\partial G\,(r)}{\partial r}\dot{r}\bar{\boldsymbol{\sigma}} \tag{27}$$

where $\boldsymbol{\varepsilon}$ is the strain tensor and $\boldsymbol{C}^0$ the initial elastic stiffness tensor. By substituting Eq. (24) into Eq. (27), one can obtain the constitutive equation of the anisotropic damage material model in the form

$$\dot{\boldsymbol{\sigma}} = \boldsymbol{C}^d:\dot{\boldsymbol{\varepsilon}} \tag{28}$$

where the damage tangent stiffness tensor $\boldsymbol{C}^d$ is expressed as

$$\boldsymbol{C}^d = (1-d)\,\boldsymbol{C}^0 - \frac{1}{H^{**}}\frac{\mathrm{d}G}{\mathrm{d}r}\bar{\boldsymbol{\sigma}}\otimes\frac{\mathrm{d}\tau^*}{\mathrm{d}\bar{\boldsymbol{\sigma}}^*}:\boldsymbol{A}^{\bar{\sigma},d}:\boldsymbol{C}^0. \tag{29}$$

The evolutionary character of the transformation tensor $\boldsymbol{A}$ is manifested by its dependence on r (or equivalently on d) as indicated in Eq. (21).

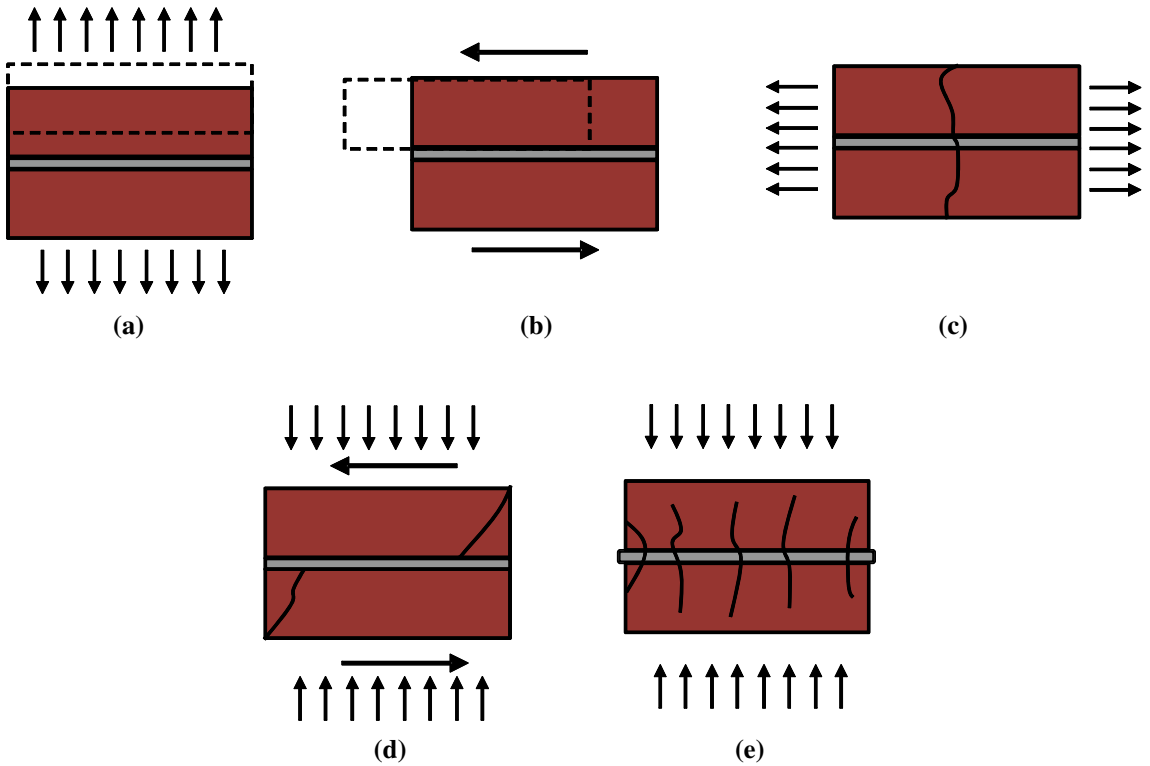

Fig. 2 Masonry failure mechanisms [4]: **a** joint tensile cracking; **b** joint slipping; **c** unit direct tensile cracking; **d** unit diagonal tensile cracking; **e** masonry crushing

3 Formulation of an orthotropic plastic–damage model for masonry

3.1 Failure modes of masonry material and corresponding damage variables

A reliable model for masonry should include all the basic types of failure mechanisms that characterize masonry, namely (a) cracking of the joints, (b) sliding along the bed or head joints at low values of normal stress, (c) cracking of the units in direct tension, (d) diagonal tensile cracking of the units at values of normal stress sufficient to develop friction in the joints, and (e) "masonry crushing", commonly identified with splitting of units in tension as a result of mortar dilatancy at high values of normal stress, as shown in Fig. 2 [4].

In marco-modelling analyses of masonry structures, irreversible processes such as slipping, cracking, and crushing cannot be described on element scale since units and joints are not individually modelled in a continuous framework. In such a framework, internal variables, such as plastic strain tensor and damage variables, are adopted in a form that they can describe the major failure mechanisms of the masonry material.

Currently, damage variables of high-rank tensors are not widely used due to high computational cost. The most common damage constitutive models for quasi-brittle materials are still isotropic damage models using two scalar damage variables, d^+ and d^-, to describe tensile and compressive damage, respectively [11,12,40,41]. This work also adopts two scalar damage variables d^+ and d^-, and by using the evolutionary linear transformation method, strengths in directions perpendicular and parallel to a joint are assigned with different values, even if the damage constitutive model is isotropic. Therefore, in view of Fig. 2, the following conclusions can be made:

(i) Failure modes (a) and (c) can be described by the tensile damage variable d^+.
(ii) Failure mode (e) can be described by the compressive damage variable d^-.
(iii) Failure mode (d) can be described by the compressive damage variable d^-, by coupling shear stress and normal stress.

However, failure mode (b), which is often referred to as "Mode II failure", cannot be described with just tensile and compressive variables d^+ and d^- since its slipping mechanism is totally different from cracking or crushing mechanisms. According to the theory of internal variables, irreversible processes of different

failure mechanisms should be described with different internal variables. Additionally, compared to bed joints, slipping failure mode along the bed joints is an essential one. Therefore, a third damage variable d^{II} is proposed in the present study to describe the Mode II failure of bed joints.

Inspired by the work of Lee and Fenves [41], the following expression is proposed here for the stiffness degradation:

$$\boldsymbol{\sigma} = (1-d)\,\boldsymbol{C}^0 : \left(\boldsymbol{\varepsilon} - \boldsymbol{\varepsilon}^e\right) = (1-d)\,\bar{\boldsymbol{\sigma}} \tag{30}$$

where the damage variable d consists of d^+ and d^- as in [38] as well as of d^{II} and is expressed in the form

$$d = 1 - \left(1-d^{\mathrm{II}}\right)\left(1-sd^+\right)\left(1-d^-\right) \tag{31}$$

with

$$s = s^0 + \left(1-s^0\right) r\left(\bar{\boldsymbol{\sigma}}\right), \tag{32}$$

$$r\left(\bar{\boldsymbol{\sigma}}\right) = \begin{cases} 0, & \text{if } \widehat{\bar{\boldsymbol{\sigma}}} = \mathbf{0} \\ \dfrac{\sum_{i=1}^{3}\left\langle\hat{\bar{\sigma}}_i\right\rangle}{\sum_{i=1}^{3}\left|\hat{\bar{\sigma}}_i\right|}, & \text{otherwise.} \end{cases} \tag{33}$$

In the above, $\hat{\bar{\sigma}}_i$ is the ith principal stress of the effective stress tensor $\bar{\boldsymbol{\sigma}}$, and the ramp function indicated by the Macaulay brackets $\langle\rangle$ returns the value of the enclosed expression if positive, but sets a zero value if negative.

3.2 Thermodynamic considerations

In this Subsection the proposed damage model defined by Eq. (31) is shown to have a sound thermodynamic basis. The procedure is analogous to that in [41]. Assume the internal energy e to be composed of an explicit part e^e and an implicit part e^i, i.e. $e = e^e + e^i$ and hence

$$\dot{e} = \dot{e}^e + \dot{e}^i. \tag{34}$$

The implicit part e^i is introduced to explain the stiffness recovery in the thermodynamic sense, while the explicit part e^e is the internal energy in the classical approach. The Helmholtz free energy ψ is therefore defined on the basis of e^e and has the form

$$\psi = e^e - sT \tag{35}$$

where s is the entropy per unit volume and T is the absolute temperature. The implicit internal energy rate balances a portion of the stress power,

$$\dot{e}^i = \omega\boldsymbol{\sigma} : \dot{\boldsymbol{\varepsilon}}, \tag{36}$$

where ω is a parameter such that $0 \le \omega \le 1$. Differentiating Eq. (35) with respect to time gives

$$\dot{\psi} = \dot{e} - \dot{e}^i - \dot{T}s - T\dot{s}. \tag{37}$$

The Helmholtz free energy for the damaged material is written as

$$\psi = \left(1-\bar{d}\right)\psi^0 \tag{38}$$

where ψ^0 is the Helmholtz free energy for the undamaged material, and $\bar{d}$ represents the unrecoverable damage in the elastic stiffness, which is defined as

$$\bar{d} = 1 - \left(1-d^{\mathrm{II}}\right)\left(1-d^+\right)\left(1-d^-\right). \tag{39}$$

Since only elastic Helmholtz free energy is considered in the present paper, ψ^0 is expressed as

$$\psi^0 = \psi^{e,0} = \frac{1}{2}\boldsymbol{\varepsilon}^e : \boldsymbol{C}^0 : \boldsymbol{\varepsilon}^e. \tag{40}$$

The Clausius–Duhem inequality is expressed as

$$D = \boldsymbol{\sigma} : \dot{\boldsymbol{\varepsilon}} - \dot{\psi} - s\dot{T} - \boldsymbol{q} \cdot \frac{\operatorname{grad}(T)}{T} \geq 0 \tag{41}$$

where $\boldsymbol{q}$ is the heat flow-vector. Substituting Eqs. (34), (35), and (36) into (41) yields

$$D = -\dot{\psi} - \dot{T}s + (1-\omega)\,\boldsymbol{\sigma} : \dot{\boldsymbol{\varepsilon}} - \boldsymbol{q}\frac{\operatorname{grad}(T)}{T} \geq 0 \tag{42}$$

which with the aid of Eqs. (39) and (40) takes the form

$$D = \left[(1-\omega)\,\boldsymbol{\sigma} - \left(1-\bar{d}\right)\frac{\partial \psi^0}{\partial \boldsymbol{\varepsilon}^e}\right] : \boldsymbol{\varepsilon}^e + (1-\omega)\,\boldsymbol{\sigma} : \boldsymbol{\varepsilon}^p + \dot{\bar{d}}\psi^0 \geq 0. \tag{43}$$

In Eq. (43), $(1-\omega)\,\boldsymbol{\sigma} : \boldsymbol{\varepsilon}^p \geq 0$ because of the convexity of the plastic potential function and $\dot{\bar{d}}\psi^0 \geq 0$ since $\dot{\bar{d}}$ and ψ^0 are positive. Therefore, in order for Eq. (43) to be satisfied, relation

$$\boldsymbol{\sigma} = \left(\frac{1-\bar{d}}{1-\omega}\right)\frac{\partial \psi^0}{\partial \boldsymbol{\varepsilon}^e} \tag{44}$$

is required to hold true as a sufficient condition. Assuming the value of ω to be

$$\omega = \frac{1 - sd^+}{1 - d^+} \tag{45}$$

and by substituting Eq. (45) into (44) one finally obtains

$$\boldsymbol{\sigma} = (1-d)\,\boldsymbol{C}^0 : \left(\boldsymbol{\varepsilon} - \boldsymbol{\varepsilon}^e\right) = \left(1-d^{\mathrm{II}}\right)\left(1-sd^+\right)\left(1-d^-\right)\bar{\boldsymbol{\sigma}} \tag{46}$$

which coincides with Eqs. (30)–(33). Thus, it has been proven that the adopted expression of Eqs. (30)–(33) has a sound thermodynamic basis.

3.3 Plastic evolution

In this model, a Rankine yield criterion for tension and a Drucker–Prager yield criterion for compression are adopted as the known isotropic yield criteria. By using the evolutionary linear transformation methodology discussed above, these isotropic yield criteria are extended to anisotropic ones with both initial and evolutionary anisotropy. A plastic model is thus obtained, which is almost the same as the one in Lourenço's work [4], but without directly rewriting the isotropic Rankine and Drucker–Prager yield functions as Lourenço did.

(i) Plastic yield criterion for tension

The Rankine yield criterion for tension is expressed as

$$F^{t*}\left(\bar{\boldsymbol{\sigma}}^*, \kappa^t\right) = \left\langle \hat{\bar{\sigma}}_1{}^* \right\rangle - \bar{f}^{t*} \tag{47}$$

where κ^t is the hardening variable in tension and $\bar{f}^{t*}$ is the isotropic uniaxial tensile yielding threshold for effective stress. Following a procedure similar to that in [4], Eq. (47) is also written in the form

$$F^{t*}\left(\bar{\boldsymbol{\sigma}}^*, \kappa^t\right) = \left(\frac{1}{2}\bar{\boldsymbol{\sigma}}^* : \boldsymbol{M}^{pt*} : \bar{\boldsymbol{\sigma}}^*\right)^{\frac{1}{2}} + \frac{1}{2}\boldsymbol{\pi}^* : \bar{\boldsymbol{\sigma}}^* - \bar{f}^{t*} \tag{48}$$

where the rank-four tensor $\boldsymbol{M}^{pt*}$ has the following components in plane stress,

$$\begin{aligned} &M^{pt*}_{1111} = 0.5,\ M^{pt*}_{2222} = 0.5,\ M^{pt*}_{1212} = 1,\ M^{pt*}_{2121} = 1,\\ &M^{pt*}_{1122} = -0.5,\ M^{pt*}_{2211} = -0.5,\ M^{pt*}_{\text{else}} = 0, \end{aligned} \tag{49}$$

and the rank-two tensor $\boldsymbol{\pi}^*$ is expressed as

$$\pi^*_{11} = 1,\ \ \pi^*_{12} = 0,\ \pi^*_{21} = 0,\ \pi^*_{22} = 1. \tag{50}$$

Since the softening behaviour of the material will be considered in the damage correction part of the constitutive model in Sect. 3.4, in the plastic correction part considered here one only deals with the hardening behaviour. Therefore, $\bar{f}^{t*}$ is assumed to be a linear function of κ^t of the form

$$\bar{f}^{t*}\left(\kappa^t\right) = \bar{f}^{0t*} + E^{pt*}\kappa^t \tag{51}$$

where $\bar{f}^{0t*}$ is the initial value of $\bar{f}^{t*}$, and E^{pt*} is the isotropic tensile hardening modulus defined as

$$E^{pt*} = \frac{\mathrm{d}\bar{f}^{t*}}{\mathrm{d}\kappa^t} \tag{52}$$

An associated flow rule is adopted for the tensile condition meaning that

$$F^{pt*}\left(\bar{\boldsymbol{\sigma}}^*, \kappa^t\right) = F^{t*}\left(\bar{\boldsymbol{\sigma}}^*, \kappa^t\right) = \left(\frac{1}{2}\bar{\boldsymbol{\sigma}}^* : \boldsymbol{M}^{pt*} : \bar{\boldsymbol{\sigma}}^*\right)^{\frac{1}{2}} + \frac{1}{2}\boldsymbol{\pi}^* : \bar{\boldsymbol{\sigma}}^*. \tag{53}$$

Next, the rank-four transformation tensor $\boldsymbol{A}^{\bar{\sigma},pt}$ is introduced, which includes information for the orthotropic tensile behaviour of the masonry material. In this Section, the expression of the transformation tensor is given for a plane stress condition, but its extension towards a three-dimensional condition is quite straightforward. Thus, in a material coordinate system denoted by axes 1 and 2, the components of $\boldsymbol{A}^{\bar{\sigma},pt}$ are of the form [33]

$$\begin{aligned} &A^{\bar{\sigma},pt}_{1111} = \bar{f}^{t*}/\bar{f}^t_{11},\ A^{\bar{\sigma},pt}_{2222} = \bar{f}^{t*}/\bar{f}^t_{22},\ A^{\bar{\sigma},pt}_{1212} = \bar{f}^{t*}/2\bar{f}^t_{12},\ A^{\bar{\sigma},pt}_{2121} = \bar{f}^{t*}/2\bar{f}^t_{12},\\ &A^{\bar{\sigma},pt}_{2112} = \bar{f}^{t*}/2\bar{f}^t_{12},\ A^{\bar{\sigma},pt}_{1221} = \bar{f}^{t*}/2\bar{f}^t_{12},\ A^{\bar{\sigma},pt}_{\text{else}} = 0, \end{aligned} \tag{54}$$

where $\bar{f}^t_{11}$, $\bar{f}^t_{22}$, and $\bar{f}^t_{12}$ are the orthotropic tensile yielding threshold values for the effective stress, which are constant in [33] but depend on plastic evolution in this work and read

$$\bar{f}^t_{ij}\left(\kappa^t\right) = \bar{f}^{0t}_{ij} + E^{pt}_{ij}\kappa^t \tag{55}$$

with $\bar{f}^{0t}_{ij}$ being the initial value of $\bar{f}^t_{ij}$, and E^{pt}_{ij} the corresponding hardening modulus expressed as

$$E^{pt}_{ij} = \frac{\mathrm{d}\bar{f}^t_{ij}}{\mathrm{d}\kappa^t} \tag{56}$$

and obtained by material tests . From Eqs. (54)–(56) one can see how all the material information is included in the transformation tensor $\boldsymbol{A}^{\bar{\sigma},pt}$. Therefore, the isotropic parameters $\bar{f}^{0t*}$ and E^{pt*} are actually fictitious parameters that can be assigned with any nonzero values.

The tensile plastic multiplier $\dot{\lambda}^{pt}$ can be calculated from Eq. (14) as

$$\dot{\lambda}^{pt} = \frac{\frac{\partial F^{t*}}{\partial \bar{\boldsymbol{\sigma}}^*} : \boldsymbol{A}^{\bar{\sigma},pt} : \boldsymbol{C}_0 : \dot{\boldsymbol{\varepsilon}}}{H^{t*}} \tag{57}$$

where explicit expressions for all the above quantities are found in "Appendix A".

(ii) Plastic yield criterion for compression

The Drucker–Prager yield criterion for compression is expressed as [42]

$$F^{c*}\left(\bar{\boldsymbol{\sigma}}^*, \kappa^c\right) = \alpha\bar{I}^*_1 + \sqrt{3\bar{J}^*_2} - (1-\alpha)\,\bar{f}^{c*} \tag{58}$$

where α is a material parameter that controls the biaxial compressive strength, $\bar{f}^{c*}$ is the isotropic uniaxial compressive yielding threshold for effective stress, $\bar{I}^*_1$ is the first invariant of $\bar{\boldsymbol{\sigma}}^*$, and $\bar{J}_2$ is the second invariant of the deviatoric tensorial components of $\bar{\boldsymbol{\sigma}}^*$. Again, since the softening behaviour of the material will be considered in the damage correction part of the constitutive model in Sect. 3.4, in the plastic correction part considered here, one only deals with the hardening behaviour. Therefore, $\bar{f}^{c*}$ is assumed to be a linear function of the hardening variable κ^c of the form

$$\bar{f}^{c*}\left(\kappa^c\right) = \bar{f}^{0c*} + E^{pc*}\kappa^c \tag{59}$$

where $\bar{f}^{0c*}$ is the initial value of $\bar{f}^{c*}$, and E^{pc*} is the isotropic compressive hardening modulus

$$E^{pc*} = \frac{\mathrm{d}\bar{f}^{c*}}{\mathrm{d}\kappa^c}. \tag{60}$$

A non-associated flow rule is adopted for the compressive condition, and thus a plastic potential function F^{pc*} is introduced of the form

$$F^{pc*}\left(\bar{\boldsymbol{\sigma}}^*, \kappa^c\right) = \alpha^p \bar{I}_1^* + \sqrt{2\bar{J}_2^*} \tag{61}$$

where α^p is a material parameter that controls the dilatancy angle. Next, the rank-four transformation tensor $\boldsymbol{A}^{\sigma,pc}$ is introduced, which includes information for the orthotropic compressive behaviour of the masonry material. The components of $\boldsymbol{A}^{\sigma,pc}$ are of the form [33]

$$\begin{aligned}
&A_{1111}^{\bar{\sigma},pc} = \bar{f}^{c*}/\bar{f}_{11}^c,\ A_{2222}^{\bar{\sigma},pc} = \bar{f}^{c*}/\bar{f}_2^c,\ A_{1212}^{\bar{\sigma},pc} = \left[(1-\alpha)\,\bar{f}^{c*}\right]/\left(2\sqrt{3}\bar{f}_{12}^c\right),\\
&A_{2121}^{\bar{\sigma},pc} = \left[(1-\alpha)\,\bar{f}^{c*}\right]/\left(2\sqrt{3}\bar{f}_{12}^c\right),\ A_{2112}^{\bar{\sigma},pc} = \left[(1-\alpha)\,\bar{f}^{c*}\right]/\left(2\sqrt{3}\bar{f}_{12}^c\right),\\
&A_{1221}^{\bar{\sigma},pc} = \left[(1-\alpha)\,\bar{f}^{c*}\right]/\left(2\sqrt{3}\bar{f}_{12}^c\right),\ A_{\text{else}}^{\bar{\sigma},pc} = 0
\end{aligned} \tag{62}$$

where $\bar{f}_{11}^c$, $\bar{f}_{22}^c$, and $\bar{f}_{12}^c$ are the orthotropic compressive yielding threshold values for effective stress, which are constant in [33] but depend on plastic evolution in this work and read

$$\bar{f}_{ij}^c\left(\kappa^c\right) = \bar{f}_{ij}^{0c} + E_{ij}^{pc}\kappa^c \tag{63}$$

with $\bar{f}_{ij}^{0c}$ being the initial value of $\bar{f}_{ij}^c$, and E^{pc*} the corresponding compressive hardening modulus defined as

$$E_{ij}^{pc} = \frac{\mathrm{d}\bar{f}_{ij}^c}{\mathrm{d}\kappa^c} \tag{64}$$

and obtained by material tests. Similar to the case of the tensile plastic criterion, here $\bar{f}^{0c*}$ and E^{pc*} are also actually fictitious parameters that can be assigned with any nonzero values. The compressive plastic multiplier $\dot{\lambda}^{pc}$ can be calculated from Eq. (14) as

$$\dot{\lambda}^{pc} = \frac{\frac{\partial F^{c*}}{\partial \bar{\boldsymbol{\sigma}}^*} : \boldsymbol{A}^{\bar{\sigma},pc} : \boldsymbol{C}_0 : \dot{\boldsymbol{\varepsilon}}}{H^{c*}} \tag{65}$$

where explicit expressions for all the above quantities are found in "Appendix B".

One can introduce the material parameters $\bar{k}_{11}^c$ and $\bar{k}_{22}^c$ of the form

$$\bar{k}_{11}^c = \frac{\bar{f}^{bc}\left(\kappa^c\right)}{\bar{f}_{11}^c\left(\kappa^c\right)},\quad \bar{k}_{22}^c = \frac{\bar{f}^{bc}\left(\kappa^c\right)}{\bar{f}_{22}^c\left(\kappa^c\right)} \tag{66}$$

representing the ratios of the biaxial compressive strength over the uniaxial compressive strengths under the same plastic evolution level described by κ^c. Even though the values of $\bar{k}_{11}^c$ and $\bar{k}_{22}^c$ may change with the process of plastic evolution as shown in Eq. (66), the simplifying assumption is made here that $\bar{k}_{11}^c$ and $\bar{k}_{22}^c$ are constant and equal to the initial yielding strength ratios,

$$\bar{k}_{11}^c = \frac{\bar{f}^{0bc}}{\bar{f}_{11}^{0c}},\quad \bar{k}_{22}^c = \frac{\bar{f}^{0bc}}{\bar{f}_{22}^{0c}}. \tag{67}$$

Then, the material parameter α in Eq. (58) can be expressed as

$$\alpha = \frac{\sqrt{\left(\bar{k}_{11}^c\right)^2 + \left(\bar{k}_{22}^c\right)^2 - \bar{k}_{11}^c\bar{k}_{22}^c} - 1}{\bar{k}_{11}^c + \bar{k}_{22}^c - 1}. \tag{68}$$

(iii) A composite yield criterion

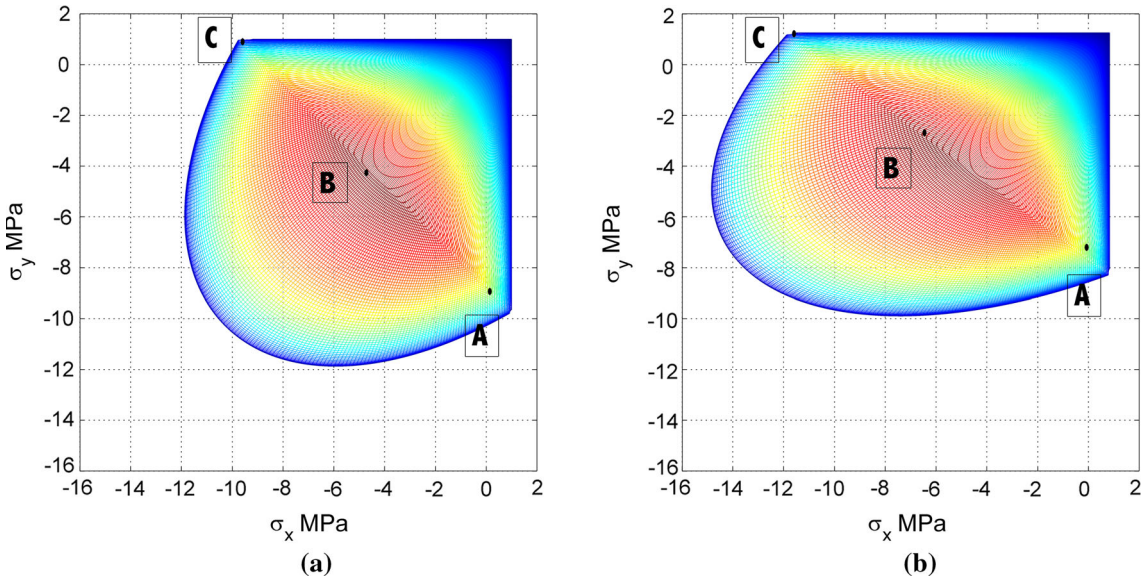

Fig. 3 Composite yield surfaces for plane stress conditions in stress space: **a** isotropic yield surface; **b** orthotropic yield surface

Combining the tensile and compressive yield criteria previously defined, one can construct a composite yield criterion as shown in Fig. 3, where the known isotropic yield surface (a) and the orthotropic yield surface (b) obtained by using the transformation method are compared. As it can be seen, the values of yield strengths in different material directions can be totally different for the orthotropic yield surface (b), although they are the same for the isotropic yield surface (a).

At the intersection of two surfaces of a composite yield surface, like those indicated by points A, B, C in Fig. 3, the plastic strain rate $\dot{\boldsymbol{\varepsilon}}^p$ is obtained from a linear combination of the plastic strain rates of the two yield surfaces, reading

$$\dot{\boldsymbol{\varepsilon}}^p = \dot{\boldsymbol{\varepsilon}}^{pt} + \dot{\boldsymbol{\varepsilon}}^{pc} = \dot{\lambda}^{pt} \frac{\partial F^{pt}}{\partial \bar{\boldsymbol{\sigma}}} + \dot{\lambda}^{pc} \frac{\partial F^{pc}}{\partial \bar{\boldsymbol{\sigma}}}. \tag{69}$$

The consistency condition can be written as

$$\dot{\lambda}^{p\alpha} = \sum_{\beta \in \{t,c\}} h^{\alpha\beta} \left(\frac{\partial F^{\beta}}{\partial \bar{\boldsymbol{\sigma}}} : \boldsymbol{C}^0 : \dot{\boldsymbol{\varepsilon}} \right), \quad \alpha \in \{t, c\}, \tag{70}$$

and the plastic tangent stiffness tensor can be expressed as

$$\boldsymbol{C}^{ep} = \boldsymbol{C}^0 - \sum_{\alpha,\beta \in \{t,c\}} h^{\alpha\beta} \left(\boldsymbol{C} : \frac{\partial F^{p\alpha}}{\partial \bar{\boldsymbol{\sigma}}} \right) \otimes \left(\boldsymbol{C} : \frac{\partial F^{\beta}}{\partial \bar{\boldsymbol{\sigma}}} \right) \tag{71}$$

where

$$h_{\alpha\beta} = \frac{\partial F^{\alpha}}{\partial \bar{\boldsymbol{\sigma}}} : \boldsymbol{C}^0 : \frac{\partial F^{p\beta}}{\partial \bar{\boldsymbol{\sigma}}} - \frac{\partial F^{\alpha}}{\partial \boldsymbol{\kappa}} \cdot \frac{\partial \boldsymbol{\kappa}}{\partial \dot{\lambda}^{p\beta}}, \tag{72}$$

$$\sum_{\beta \in \{t,c\}} h^{\alpha\beta} h_{\beta\gamma} = \delta^{\alpha}_{\gamma}. \tag{73}$$

Readers may refer to the work of Simo and Hughes [37] for more information about composite yield surface plasticity.

3.4 Damage evolution

In this Section, the damage evolution part of the constitutive model for masonry is proposed. Since plastic strain has been dealt with in the plastic evolution part previously discussed, only effective stress, Cauchy stress, and elastic strain are left to be studied in this Section. Therefore, the upper script e of the elastic strain tensor $\boldsymbol{\varepsilon}^e$ will be omitted in this Section.

In the present damage model, the effective stress tensors obtained from the plastic correcting procedure defined in the previous Section are split into a positive part and a negative part, in order to describe the different behaviours under tension and compression. This is a strategy first proposed in the field of concrete damage models by Mazars [43] and Mazars and Pijaudier-Cabot [44] in the Cauchy stress space and by Faria et al. [12] in the effective stress space. Thus, one has

$$\begin{aligned} \bar{\boldsymbol{\sigma}}^+ &= \sum_i \left\langle \hat{\bar{\sigma}}_i \right\rangle \boldsymbol{p}_i \otimes \boldsymbol{p}_i, \\ \bar{\boldsymbol{\sigma}}^- &= \bar{\boldsymbol{\sigma}} - \bar{\boldsymbol{\sigma}}^+ \end{aligned} \tag{74}$$

where $\hat{\bar{\sigma}}_i$ is the i-th principal stress value of the effective stress tensor $\bar{\boldsymbol{\sigma}}$, while $\boldsymbol{p}_i$ represents the unit vector associated with the i-th principal direction. Equation (74) can also be expressed as

$$\begin{aligned} \bar{\boldsymbol{\sigma}}^+ &= \boldsymbol{P}^+ : \bar{\boldsymbol{\sigma}}, \\ \bar{\boldsymbol{\sigma}}^- &= \left(\boldsymbol{I} - \boldsymbol{P}^+\right) : \bar{\boldsymbol{\sigma}} \end{aligned} \tag{75}$$

where $\boldsymbol{I}$ is the rank-four identity tensor and $\boldsymbol{P}^+$ is a projection tensor of the form

$$\boldsymbol{P}^+ = \sum_i H\left(\hat{\bar{\sigma}}_i\right) \boldsymbol{p}_i \otimes \boldsymbol{p}_i \otimes \boldsymbol{p}_i \otimes \boldsymbol{p}_i \tag{76}$$

with H () denoting the Heaviside function.

(i) Damage criterion for tension

The tensile damage criterion is assumed to have the form [12,39]

$$g^+\left(\tau^+, r^+\right) = g^{+*}\left(\tau^{+*}, r^{+*}\right) = \tau^{+*} - r^{+*} \tag{77}$$

where $\tau^{+*} = \left\langle \hat{\bar{\sigma}}_1{}^{+*} \right\rangle$ is the tensile equivalent stress. Equation (77) is then expressed as

$$g^+\left(\tau^+, r^+\right) = \left(\frac{1}{2}\bar{\boldsymbol{\sigma}}^{+*} : \boldsymbol{M}^{dt*} : \bar{\boldsymbol{\sigma}}^{+*}\right)^{\frac{1}{2}} + \frac{1}{2}\boldsymbol{\pi}^* : \bar{\boldsymbol{\sigma}}^{+*} - r^{+*} \tag{78}$$

where the rank-four tensor $\boldsymbol{M}^{dt*}$ has the following components in plane stress:

$$\begin{aligned} &M^{dt*}_{1111} = 0.5,\ M^{dt*}_{2222} = 0.5,\ M^{dt*}_{1212} = 1,\ M^{dt*}_{2121} = 1, \\ &M^{dt*}_{1122} = -0.5,\ M^{dt*}_{2211} = -0.5,\ M^{dt*}_{\text{else}} = 0. \end{aligned} \tag{79}$$

The rank-two tensor $\boldsymbol{\pi}^*$ is expressed as

$$\pi^*_{11} = 1,\ \ \pi^*_{12} = 0,\ \pi^*_{21} = 0,\ \pi^*_{22} = 1, \tag{80}$$

and $r^{+*}$is the isotropic damage threshold for tension of the form [12,39]

$$r^{+*} = \max\left\{r^{0+*}, \max\left(\tau^{+*}\right)\right\} \tag{81}$$

with $r^{0+*} = r^{+*}\left(f^{0+*}\right)$ being the initial isotropic damage threshold, and f^{0+*} the initial uniaxial strength for isotropic damage threshold. For this Rankine-type threshold, one has

$$r^{0+*} = f^{0+*}. \tag{82}$$

The tensile damage variable d^+ is defined as an exponential softening function of r^{0+*} of the form [45]

$$d^+ = G^{+*}\left(r^{+*}\right) = \begin{cases} 0, & r^{+*} = r^{0+*} \\ 1 - \frac{r^{0+*}}{r^{+*}} e^{A^+\left(1-\frac{r^{+*}}{r^{0+*}}\right)}, & r^{+*} > r^{0+*}, \end{cases} \tag{83}$$

$$A^+ = \left(\frac{G_f^{+*} E^{+*}}{l_{\mathrm{ch}}\left(f^{0+*}\right)^2} - \frac{1}{2}\right)^{-1} \geq 0 \tag{84}$$

where E^{+*} is the elastic modulus for the isotropic damage constitutive model, l_{ch} is the characteristic length of the finite element, and G_f^{+*} is the tensile elastic fracture energy per unit area of the form

$$G_f^{+*} = \int_{\varepsilon^{0+*}}^{\infty} \sigma^{+*} \mathrm{d}\varepsilon \tag{85}$$

with ε^{0+*} being the elastic strain corresponding to the initial damage evolution.

Similar to the case of the plastic correcting procedure, the material information here will be included in the transformation tensor. Therefore, isotropic parameters such as f^{0+*}, $E^{+*}$and G_f^{+*} are also fictitious parameters that can be assigned with any nonzero values.

Next, the rank-four transformation tensor $\boldsymbol{A}^{\bar{\sigma},d+}$ for tensile damage is introduced. For each material direction, the relationship between the damage variable and the equivalent stress is assumed to have the same exponential softening function form as Eq. (83), i.e.

$$d_{ij}^+ = G_{ij}^+\left(r^+\right) = \begin{cases} 0, & r_{ij}^+ = r_{ij}^{0+} \\ 1 - \frac{r_{ij}^{0+}}{r_{ij}^+} e^{A_{ij}^+\left(1-\frac{r_{ij}^+}{r_{ij}^{0+}}\right)}, & r_{ij}^+ > r_{ij}^{0+} \end{cases} \tag{86}$$

where $r^+ = \bar{\sigma}_{ij}^+$, and material parameters A_{ij}^+ have the same meaning as in Eq. (84) and can be obtained by uniaxial tensile tests along each material direction. The components of A_{ij}^+ can be expressed as

$$\begin{aligned}
&A_{1111}^{\bar{\sigma},d+}\left(r^{+*}\right) = r^{+*}/\left(G_{11}^+\right)^{-1}\left[G^{+*}\left(r^{+*}\right)\right], \quad A_{2222}^{\bar{\sigma},d+} = r^{+*}/\left(G_{22}^+\right)^{-1}\left[G^{+*}\left(r^{+*}\right)\right], \\
&A_{1212}^{\bar{\sigma},d+} = r^{+*}/\left\{2\left(G_{12}^+\right)^{-1}\left[G^{+*}\left(r^{+*}\right)\right]\right\}, \quad A_{2121}^{\bar{\sigma},d+} = r^{+*}/\left\{2\left(G_{12}^+\right)^{-1}\left[G^{+*}\left(r^{+*}\right)\right]\right\}, \\
&A_{2112}^{\bar{\sigma},d+} = r^{+*}/\left\{2\left(G_{12}^+\right)^{-1}\left[G^{+*}\left(r^{+*}\right)\right]\right\}, \quad A_{1221}^{\bar{\sigma},d+} = r^{+*}/\left\{2\left(G_{12}^+\right)^{-1}\left[G^{+*}\left(r^{+*}\right)\right]\right\}, \\
&A_{\mathrm{else}}^{\bar{\sigma},d+} = 0.
\end{aligned} \tag{87}$$

(ii) Damage criterion for compression

The compressive isotropic equivalent stress is defined by a combination of octahedral normal stress $\hat{\bar{\boldsymbol{\sigma}}}_{oct}^*$ and octahedral shear stress $\hat{\bar{\boldsymbol{\tau}}}_{oct}^*$ of the form [12]

$$\bar{\tau}^{-*} = \sqrt{3}(K\hat{\bar{\boldsymbol{\sigma}}}_{oct}^* + \hat{\bar{\boldsymbol{\tau}}}_{oct}^*). \tag{88}$$

One can introduce the material parameters $\bar{k}_{11}^-$ and $\bar{k}_{22}^-$ of the form

$$\bar{k}_{11}^- = \frac{\bar{f}^{b-}\left(r^{-*}\right)}{\bar{f}_{11}^-\left(r^{-*}\right)}, \quad \bar{k}_{22}^- = \frac{\bar{f}^{b-}\left(r^{-*}\right)}{\bar{f}_{22}^-\left(r^{-*}\right)} \tag{89}$$

representing the ratios of the biaxial compressive strength over the uniaxial compressive strengths under the same damage evolution level described by r^{-*}. Even though the values of $\bar{k}_{11}^-$ and $\bar{k}_{22}^-$ may change with the process of damage evolution, the simplifying assumption is made here that $\bar{k}_{11}^-$ and $\bar{k}_{22}^-$ are constant and equal to the initial yielding strength ratios,

$$\bar{k}_{11}^- = \frac{\bar{f}^{b-}\left(r^{0-*}\right)}{\bar{f}_{11}^-\left(r^{0-*}\right)}, \quad \bar{k}_{22}^- = \frac{\bar{f}^{b-}\left(r^{0-*}\right)}{\bar{f}_{22}^-\left(r^{0-*}\right)}. \tag{90}$$

Then, material parameter K in Eq. (88) can be expressed as

$$K = \sqrt{2}\frac{\sqrt{\left(\bar{k}_{11}^{-}\right)^2 + \left(\bar{k}_{22}^{-}\right)^2 - \bar{k}_{11}^{-}\bar{k}_{22}^{-}} - 1}{\bar{k}_{11}^{-} + \bar{k}_{22}^{-} - 1}. \tag{91}$$

The damage criterion is expressed as

$$g^{-}\left(\tau^{-}, r^{-}\right) = g^{-*}\left(\tau^{-*}, r^{-*}\right) = \tau^{-*} - r^{-*} \tag{92}$$

where r^{-*} is the isotropic damage threshold for compression defined as [12,39]

$$r^{-*} = \max\left\{r^{0-*}, \max\left(\tau^{-*}\right)\right\} \tag{93}$$

with $r^{0-*} = r^{-*}\left(f^{0-*}\right)$ being the initial isotropic damage threshold. By considering a one-dimensional loading condition and bearing Eq. (88) in mind, one has

$$r^{0-*} = \frac{\sqrt{3}}{3}\left(K - \sqrt{2}\right) f^{0-*}. \tag{94}$$

The compressive damage variable d^{-} is defined here as

$$d^{-} = G^{-*}\left(r^{-*}\right) = \begin{cases} 0, & r^{-*} < r^{0-*} \\ a^{-}\frac{r^{e}}{r}\left(\frac{r^{-*}-r^{0-*}}{r^{p-*}-r^{0-*}}\right)^2, & r^{0-*} \le r^{-*} \le r^{p-*}, \\ 1 - \frac{r^{e-*}}{r^{-*}}\operatorname{sech}^2\left(b^{-}\left(\frac{r^{-*}}{r^{p-*}} - 1\right)\right), & r^{-*} \ge r^{p-*} \end{cases} \tag{95}$$

$$a^{-} = \frac{r^{p-} - r^{e-}}{r^{e-}}, \quad b^{-} = \frac{3r^{e-*}r^{p-*}}{\left(\sqrt{2} - K\right)^2 g'^{-*}E^{-*}}, \tag{96}$$

$$g'^{-*} = \frac{G_f'^{-*}}{l_{\mathrm{ch}}}, \tag{97}$$

$$r^{e-*} = r^{-*}(f^{e-*}), \quad r^{p-*} = r^{-*}(f^{p-*}) \tag{98}$$

with f^{e-*} being the compressive peak strength, ε^{p-*} the elastic strain under uniaxial compressive stress f^{e-*}, f^{p-*} the value of uniaxial effective stress corresponding to elastic strain ε^{p-*} of the form $f^{p-*} = E^{-*}\varepsilon^{p-*}$, and with isotropic damage threshold values r^{e-*} and r^{p-*} corresponding to f^{e-*} and f^{p-*}, respectively. Figure 4 shows the physical definition of material parameters f^{0-*}, f^{e-*}, f^{p-*}, and $G_f'^{-*}$. It is worth noting that $G_f'^{-*}$ is a redefined elastic facture energy that corresponds to the local contribution of the stress–strain curve, i.e.

$$G_f^{-*} = \int_{\varepsilon^{p-*}}^{\infty} \sigma^{-*}\mathrm{d}\varepsilon. \tag{99}$$

However, there is still no definite conclusion about whether compressive failure is a local mechanism. If not, the value of l_{ch} in Eq. (97) should no longer be decided according to the size of the finite elements, but according to the size of the actual damage zone, as in Sect. 5.1.

Finally, the rank-four transformation tensor $\boldsymbol{A}^{\bar{\sigma},d-}$ for compressive damage is introduced. The components of $\boldsymbol{A}^{\bar{\sigma},d-}$ can be calculated from Eq. (87) by simply replacing the plus sign (+) by the minus sign (−) everywhere.

(iii) Damage criterion for Mode II failure of bed joints

The damage criterion for Mode II failure of bed joints is assumed to have the Coulomb friction form used in micro-models [4], i.e.

$$g^{\mathrm{II}}(\tau^{\mathrm{II}}, r^{\mathrm{II}}) = \tau^{\mathrm{II}} - r^{\mathrm{II}} \le 0, \tag{100}$$

$$r^{\mathrm{II}} = \max\left[r^{0,\mathrm{II}}, \max(\tau^{\mathrm{II}})\right] \tag{101}$$

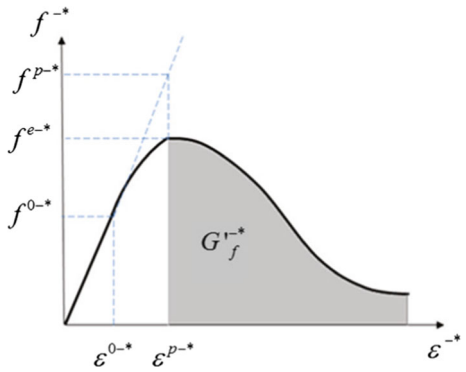

Fig. 4 Material parameters in compressive isotropic damage model

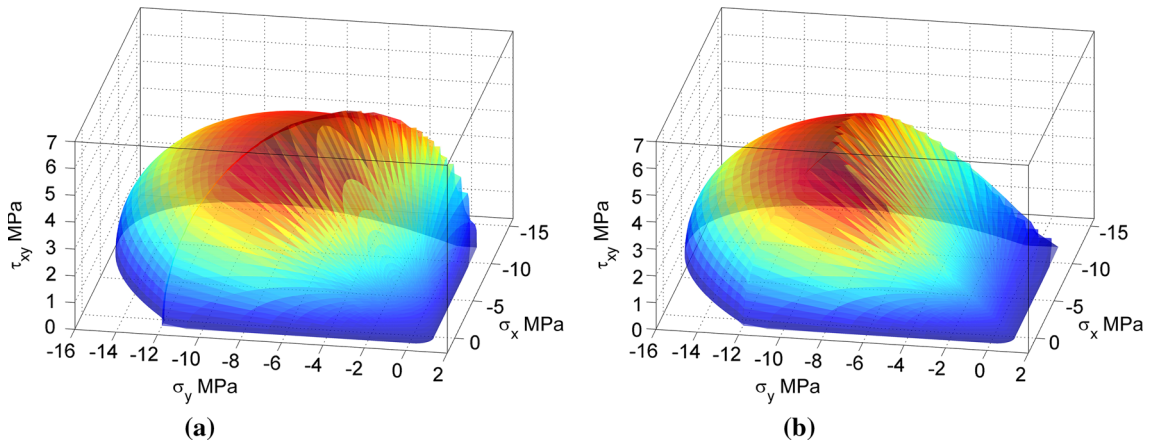

Fig. 5 Damage threshold surfaces without (**a**) and with (**b**) considering the Mode II failure of bed joints

where $r^{0,\mathrm{II}}$ is the initial equivalent stress threshold determined by shearing tests and the equivalent stress τ^{II} is given in terms of the shear stress $\bar{\sigma}_{12}$ along the bed joint, the normal stress $\bar{\sigma}_{22}$ perpendicular to the bed joint and the corresponding friction angle ϕ^{II} as

$$\tau^{\mathrm{II}} = |\bar{\sigma}_{12}| + \bar{\sigma}_{22} \tan \phi^{\mathrm{II}}. \tag{102}$$

The softening stress–strain relationship in the Mode II failure of the bed joint can be defined as an exponential function [4]. Thus, the Mode II damage variable d^{II} is assumed to be of the form

$$d^{\mathrm{II}} = G^{\mathrm{II}}(r^{\mathrm{II}}) = 1 - \frac{r^{0,\mathrm{II}}}{r^{\mathrm{II}}} e^{B^{\mathrm{II}}\left(1-\frac{r^{\mathrm{II}}}{r^{0,\mathrm{II}}}\right)}, \quad r^{\mathrm{II}} \geq r^{0,\mathrm{II}}, \tag{103}$$

$$B^{\mathrm{II}} = \left(\frac{G_f^{\mathrm{II}} G_{12}}{l_{\mathrm{ch}} \left(f_{12}^{\mathrm{II}}\right)^2} - \frac{1}{2} \right)^{-1} \geq 0 \tag{104}$$

where G_f^{II} is the fracture energy per unit area for Mode II failure and G_{12} is the shearing modulus. Damage threshold surfaces with and without considering the Mode II failure of bed joints are shown in Fig. 5.

4 Finite element implementation

4.1 Programming interface with commercial FEM software

The proposed inelastic anisotropic material model, which is capable of simulating the material behaviour under any kind of monotonic or cyclic loading, has been implemented into the commercial finite element code

ANSYS [46] with the aid of the UserMat subroutine that defines the material stress–strain relationship. Thus one can use ANSYS to analyse any structure exhibiting this material behaviour to any kind of loading.

During the solution phase, the subroutine is called at every material integration point of the elements. ANSYS passes in stresses, strains, and state variable values at the beginning of the time increment and strain increment at the current increment, then updates the stresses and state variables to the appropriate values at the end of the time increment. Additionally, UserMat must also provide the material Jacobian matrix, which is the matrix representation of the tangent stiffness tensor needed to describe the inelastic constitutive equation. Details about the computation of this tensor are given in the next Subsection.

In the present study, the UserMat subroutine is programmed for the plane stress condition, and masonry panels and walls are simulated by using shell elements. Of course, we could have used plane stress elements, which are simpler, instead of shell elements, which are more complicated as considering both plane stress and plate bending. Shell elements were adopted here for the convenience of future extensions/applications involving three-dimensional deformation patterns.

4.2 Tangent stiffness tensor computation

In numerical nonlinear analyses of materials with softening behaviour, a Newton–Raphson algorithm is usually employed. Therefore, the formulation of the tangent stiffness tensor is of great importance. Taking a temporal derivative of Eq. (30), one obtains

$$\dot{\boldsymbol{\sigma}} = (1-d)\,\dot{\bar{\boldsymbol{\sigma}}} - \dot{d}\bar{\boldsymbol{\sigma}} = [(1-d)\,\boldsymbol{I} - \boldsymbol{R}] : \dot{\bar{\boldsymbol{\sigma}}} \tag{105}$$

where $\boldsymbol{R}$ is a rank-four tensor such that

$$\dot{d}\bar{\boldsymbol{\sigma}} = \boldsymbol{R} : \dot{\bar{\boldsymbol{\sigma}}}, \tag{106}$$

and $\dot{d}$ is obtained from Eq. (31) and has the form

$$\dot{d} = \dot{d}'\left(1-d^{\mathrm{II}}\right) + \dot{d}^{\mathrm{II}}\left(1-d'\right) \tag{107}$$

with

$$\dot{d}' = \left(1-d^{-}\right)\left(s\dot{d}^{+} + \dot{s}d^{+}\right) + \left(1-sd^{+}\right)\dot{d}^{-}. \tag{108}$$

Quantities $\dot{d}^{+}$, $\dot{d}^{-}$, $\dot{s}$, and d^{II} of Eqs. (107) and (108) are treated separately, and their computation is found in "Appendix C".

Substituting Eqs. (121)–(130) into Eq. (107) enables one to determine $\boldsymbol{R}$ from Eq. (106). Thus, the tangent stiffness tensor $\boldsymbol{C}^{\tan}$ is expressed as

$$\boldsymbol{C}^{\tan} = \frac{\mathrm{d}\boldsymbol{\sigma}}{\mathrm{d}\boldsymbol{\varepsilon}} = \frac{\mathrm{d}\boldsymbol{\sigma}}{\mathrm{d}\bar{\boldsymbol{\sigma}}} : \frac{\mathrm{d}\bar{\boldsymbol{\sigma}}}{\mathrm{d}\boldsymbol{\varepsilon}} = [(1-d)\,\boldsymbol{I} - \boldsymbol{R}] : \boldsymbol{C}^{ep} \tag{109}$$

where $\boldsymbol{C}^{ep}$ is the plastic tangent stiffness tensor defined in Eq. (71).

5 Validation of the proposed damage model

5.1 Masonry panel under cyclic compressive load

In this Subsection, the capability of the proposed model to reproduce the behaviour of masonry under cyclic load is demonstrated by a comparison of simulation results with experimental ones obtained by Nazar and Sinha [47,48] on masonry panels subjected to in-plane loading conditions. Nazar and Sinha [47,48] investigated experimentally the behaviour of brick masonry panels under uniaxial cyclic compressive loading with different bed joint orientation utilizing 45 specimens. Figure 6 shows such a masonry panel with dimensions 0.5 m×0.5 m under compression with different bedding angles θ.

The panel is modelled by one and four shell finite elements with the same material parameters, which means that the value of l_{ch} in Eq. (97) is assumed to be equal to 0.5 m for both discretizations. The results are found to be almost identical due to the uniform load distribution pattern. The analysis is completed by using 1000 equal load steps, and a Newton–Raphson method to solve the nonlinear system of equations. Convergence is attained when the ratio between the norm of the iterative residual forces and the norm of the total external forces is

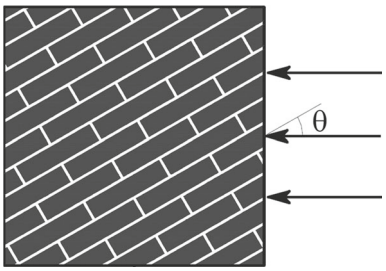

Fig. 6 A masonry panel under compression with bedding angle θ

Table 1 Material parameters for cyclic compressive test

Material parameters			
$E_1 = E^* = E'$	9700 MPa	ε_{11}^{p-}	3×10^{-3}
E_2	12,000 MPa	ε_{12}^{p-}	3×10^{-3}
$\upsilon_{12} = \upsilon^*$	0.15	ε_{22}^{p-}	2.75×10^{-3}
υ_{21}	0.12	E_{11}^{p}	7401 MPa
G_{12}	6000 MPa	E_{12}^{p}	5400 MPa
$f_{11}^{e-} = f^{e-*}$	12.11 MPa	E_{22}^{p}	8400 MPa
f_{22}^{e-}	13.92 MPa	$G_{f,1}^{\prime-} = G_f^{\prime-*}$	3500 J/m^2
f_{12}^{e-}	4.80 MPa	$G_{f,2}^{\prime-}$	4000 J/m^2
ε_{11}^{0-}	6.3×10^{-4}	$G_{f,12}^{\prime-}$	3200 J/m^2
ε_{12}^{0-}	1.32×10^{-4}	$r^{0,\mathrm{II}}$	0.75 Mpa
ε_{22}^{0-}	7.2×10^{-4}	$\tan\phi$	0.6

lower than 1%. Material parameters are listed in Table 1. Some of them were explicitly given in [47,48], while the rest were obtained indirectly from the experimental curves.

Figure 7 shows a very good agreement between the numerical and the experimental stress–strain curves for the cases of loading direction at $\theta = 0°$, 22.5°, 45°, 67.5°, and 90° with the bed joint direction. It is remarkable how successfully completely different linear, hardening, and softening behaviours of the material along different directions can be simulated by using the different transformation tensors for different domains of stress and strain spaces. It is worth noting that at $\theta = 22.5°$ the strength of the material is very low, which is due to the Mode II failure along the bed joint, thereby demonstrating the importance of this failure mode, which is considered and successfully simulated in this work.

5.2 Masonry shear wall tests

In order to further validate the proposed constitutive model, a shear wall test conducted by Raijmakers and Vermeltfoort [49] is simulated. Two brick walls with a central opening denoted J2G and J3G, as shown in Fig. 8, are considered here. These walls have dimensions 990 × 1000 mm^2, and are subjected to an initial uniform vertical load $p = 0.3$ N/mm^2 followed by a horizontal concentrated monotonically increasing load P in a way precluding any vertical displacement. The material properties of the two walls are the same and are listed in Table 2.

The failure patterns of the shear walls after loading are shown in Fig. 8. Diagonal cracks appear initially at the two corners of the opening and propagate up to the top and bottom of the wall. Additionally, tensile cracks appear at the vertical external sides of the wall involving the two piers next to the opening. Such cracks occur at the top of the left pier and at the bottom of the right one.

In this work, the wall is modelled with 4-node shell elements with an average size of 0.01 m × 0.01 m, and a value of l_{ch} in Eq. (97) equal to 0.01 m is assumed. The analysis is completed by using 1000 equal load steps, and a Newton–Raphson method to solve the nonlinear system of equations. Convergence is attained when the ratio between the norm of the iterative residual forces and the norm of the total external forces is lower than 5%.

Figure 9 depicts the horizontal reaction R versus displacement U curves obtained from tests [49] and finite element simulations including those in [9,34] and the present one. All simulations are closer to the J2G test

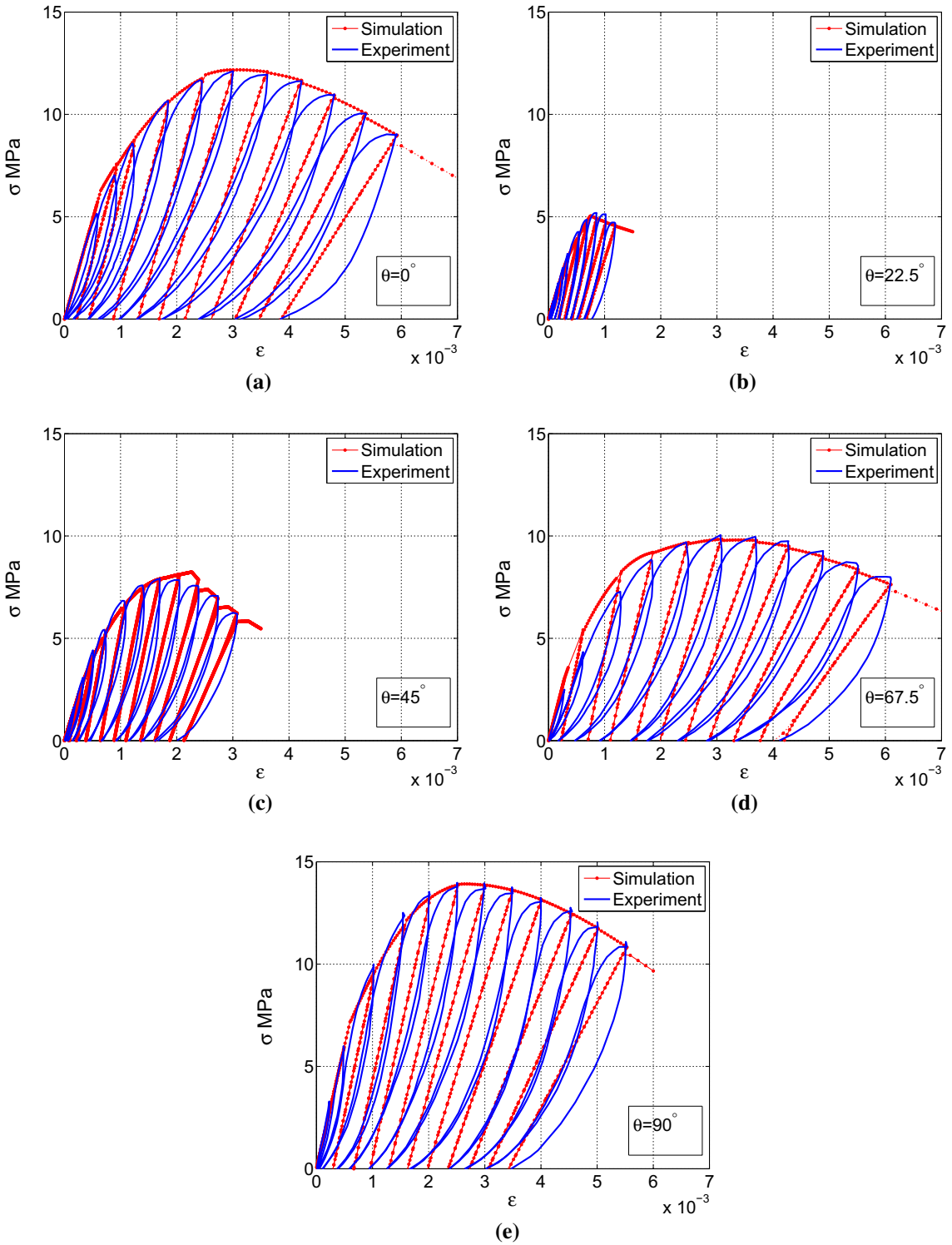

Fig. 7 Comparison of stress–strain curves obtained by the tests of Nazar and Sinha [47,48] and the numerical analyses for various angles of bed joint orientation in masonry panels under cyclic loading

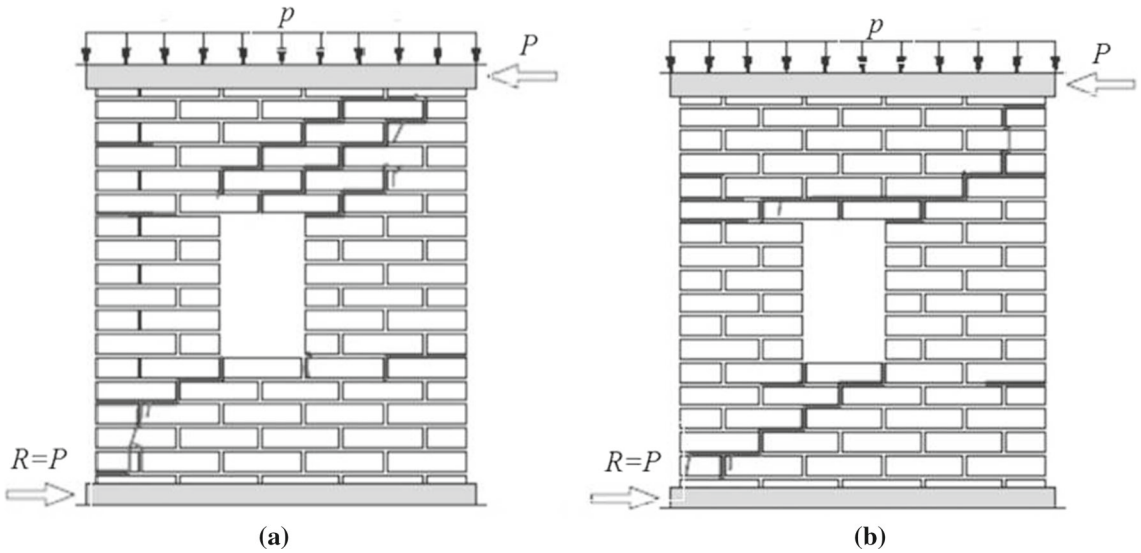

Fig. 8 Crack patterns of the walls tested by Raijmakers and Vermeltfoort [49]

Table 2 Material parameters for shear wall test

Material parameters			
$E_1 = E^* = E'$	7520 MPa	ε_{11}^{p-}	7.8×10^{-3}
E_2	3960 MPa	ε_{12}^{p-}	4.5×10^{-3}
$\upsilon_{12} = \upsilon^*$	0.09	ε_{22}^{p-}	5.6×10^{-3}
υ_{21}	0.05	E_{11}^{p}	3600 MPa
G_{12}	1460 MPa	E_{12}^{p}	740 MPa
$f_{11}^{e-} = f^{e-*}$	6.30 MPa	E_{22}^{p}	1900 MPa
f_{22}^{e-}	4.50 MPa	$G_{f,1}^{\prime-} = G_f^{\prime-*}$	20,000 J/m^2
f_{12}^{e-}	3.00 MPa	$G_{f,2}^{\prime-}$	19,400 J/m^2
f_{11}^{0-}	2.63 MPa	$G_{f,12}^{\prime-}$	11,000 J/m^2
f_{12}^{0-}	3.00 MPa	$r^{0,\mathrm{II}}$	0.9 Mpa
f_{22}^{0-}	1.50 MPa	$\tan\phi$	0.75
$f_{11}^{0+} = f^{0+*}$	0.35 MPa	$G_{f,1}^{\prime+} = G_f^{\prime+*}$	50 J/m^2
f_{22}^{0+}	0.25 MPa	$G_{f,2}^{\prime+} = G_{f,12}^{\prime+}$	48 J/m^2
f_{12}^{0+}	0.30 MPa	$G_f^{\prime\mathrm{II}}$	120 J/m^2

with the present plastic–damage simulation, and the micro-model plastic simulation of [9] is closer to that test than the elastic damage simulation of [34]. The present simulation appears to be better than the one in [34] due to the plastic evolutionary character of its transformation tensor $\boldsymbol{A}$.

Figure 10 shows the damage distribution as obtained by the present simulation for values of $P = 46.52$ kN and $P = 31.54$ kN. As can be seen by comparing Figs. 8 and 10, the orthotropic plastic–damage model proposed in the present paper is able to effectively describe the mechanical behaviour of masonry material and satisfactorily predict the failure pattern of masonry walls in plane stress.

6 Conclusions

On the basis of the preceding developments and discussion, the following conclusions can be stated:

(i) The methodology of linear stress tensor transformation for anisotropic inelastic materials has been improved by introducing an evolutionary transformation tensor that can change the values of its components according to the levels of material plasticity and damage evolutions. Thus, a new methodology for developing plasticity and damage constitutive models for anisotropic materials has been presented.

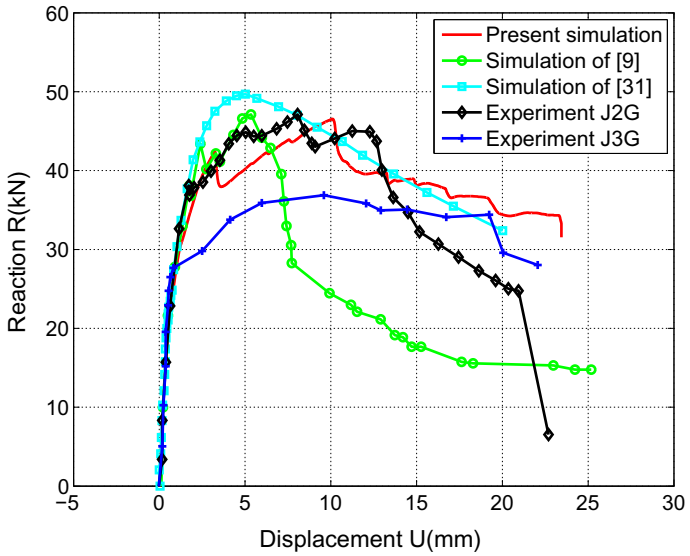

Fig. 9 Reaction–displacement curves obtained by simulation and experiments

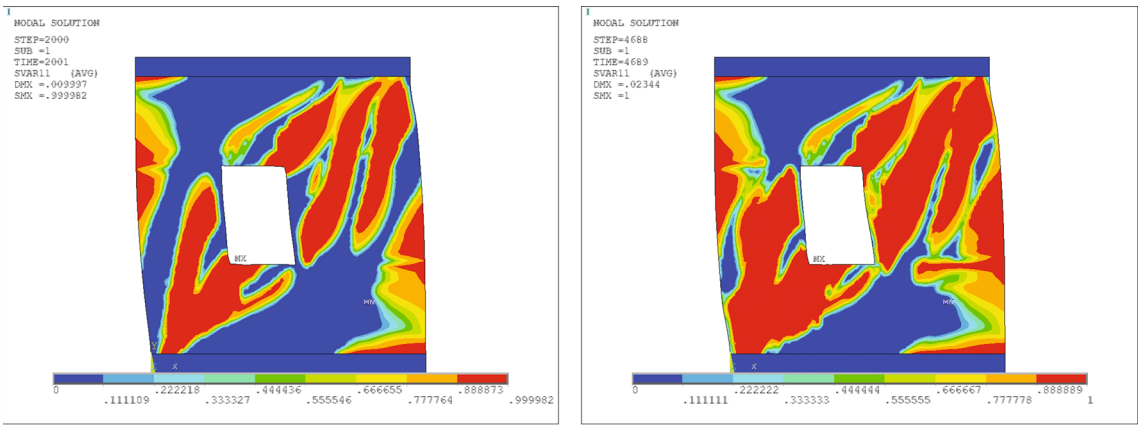

(a) for load value P=46.52kN **(b)** for load value P=31.54kN

Fig. 10 Damage distribution of masonry shear wall obtained by the present simulation

(ii) On the basis of this evolutionary linear transformation method, an orthotropic plastic–damage constitutive model for masonry materials has been developed, which is able to describe different hardening/softening behaviour along different material directions.

(iii) The additional damage variable proposed for Mode II failure, which is able to describe the slip of bed joint has been incorporated into the above described improved plastic–damage model, thereby effectively extending the applicability of macro-models.

(iv) The proposed model has been implemented into the commercial finite element code ANSYS and used for the analysis of simple masonry walls under static or cyclic loads. The numerical results were found to be in very good agreement with tests and capable of successfully describing failure modes.

(v) The proposed model has been so far applied to simple wall masonry structures. It has to be applied to masonry structures of complicated geometries, boundary conditions and loading in order to explore all of its advantages and limitations. Furthermore, the model requires many material parameters as inputs, some of which cannot easily be obtained by simple tests. Therefore, suggested values for most of the material parameters of the present model should be provided in future studies.

Appendix A: Explicit expressions for quantities in Eq. (57)

$$H^{t*} = \frac{\partial F^{t*}}{\partial \bar{\boldsymbol{\sigma}}^*} : \boldsymbol{A}^{\bar{\sigma},pt} : \boldsymbol{C}_0 : \frac{\partial F^{t*}}{\partial \boldsymbol{\sigma}^*} : \boldsymbol{A}^{\bar{\sigma},pt} - \left(\frac{\partial F^{t*}}{\partial \kappa^t} + \frac{\partial F^{t*}}{\partial \bar{\boldsymbol{\sigma}}^*} : \frac{\partial \left(\boldsymbol{A}^{\bar{\sigma},pt} \right)}{\partial \kappa^t} : \bar{\boldsymbol{\sigma}} \right) \frac{\mathrm{d}\kappa^t}{\mathrm{d}\lambda}, \tag{110}$$

$$\left[\frac{\partial A^{\bar{\sigma},pt}}{\partial \kappa^t} \right]_{1111} = \frac{E^{pt*} \bar{f}_{11}^t - E_{11}^{pt} \bar{f}^{t*}}{\left(\bar{f}_{11}^t \right)^2}, \quad \left[\frac{\partial A^{\bar{\sigma},pt}}{\partial \kappa^t} \right]_{2222} = \frac{E^{pt*} \bar{f}_2^t - E_{22}^{pt} \bar{f}^{t*}}{\left(\bar{f}_{22}^t \right)^2},$$

$$\left[\frac{\partial A^{\bar{\sigma},pt}}{\partial \kappa^t} \right]_{1212} = \frac{E^{pt*} \bar{f}_{12}^t - E_{12}^{pt} \bar{f}^{t*}}{2\left(\bar{f}_{12}^t \right)^2}, \quad \left[\frac{\partial A^{\bar{\sigma},pt}}{\partial \kappa^t} \right]_{2121} = \frac{E^{pt*} \bar{f}_{12}^t - E_{12}^{pt} \bar{f}^{t*}}{2\left(\bar{f}_{12}^t \right)^2},$$

$$\left[\frac{\partial A^{\bar{\sigma},pt}}{\partial \kappa^t} \right]_{1221} = \frac{E^{pt*} \bar{f}_{12}^t - E_{12}^{pt} \bar{f}^{t*}}{2\left(\bar{f}_{12}^t \right)^2}, \quad \left[\frac{\partial A^{\bar{\sigma},pt}}{\partial \kappa^t} \right]_{2112} = \frac{E^{pt*} \bar{f}_{12}^t - E_{12}^{pt} \bar{f}^{t*}}{2\left(\bar{f}_{12}^t \right)^2},$$

$$\left[\frac{\partial A^{\bar{\sigma},pt}}{\partial \kappa^t} \right]_{\text{else}} = 0, \tag{111}$$

$$\frac{\partial F^{t*}}{\partial \bar{\boldsymbol{\sigma}}^*} = \frac{\boldsymbol{M}^{pt*} : \bar{\boldsymbol{\sigma}}^*}{2\left(\frac{1}{2} \bar{\boldsymbol{\sigma}}^* : \boldsymbol{M}^{pt*} : \bar{\boldsymbol{\sigma}}^* \right)^{\frac{1}{2}}} + \frac{1}{2} \boldsymbol{\pi}^*, \tag{112}$$

$$\frac{\partial F^t}{\partial \kappa^t} = \frac{\partial F^{t*}}{\partial \kappa^t} + \frac{\partial F^{t*}}{\partial \bar{\boldsymbol{\sigma}}^*} : \frac{\partial \boldsymbol{A}^{\bar{\sigma},pt}}{\partial \kappa^t} : \bar{\boldsymbol{\sigma}}, \tag{113}$$

$$\frac{\partial F^{t*}}{\partial \kappa^t} = -E^{pt*} \frac{\partial F^{t*}}{\partial \bar{\boldsymbol{\sigma}}^*} : \boldsymbol{\pi}^*, \tag{114}$$

and the hardening variable κ^t is defined as

$$\dot{\kappa}^t = \dot{\lambda}^{pt}. \tag{115}$$

Appendix B: Explicit expressions for quantities in Eq. (65)

$$H^{c*} = \frac{\partial F^{c*}}{\partial \bar{\boldsymbol{\sigma}}^*} : \boldsymbol{A}^{\bar{\sigma},pc} : \boldsymbol{C}_0 : \frac{\partial F^{c*}}{\partial \boldsymbol{\sigma}^*} : \boldsymbol{A}^{\bar{\sigma},pc} - \left(\frac{\partial F^{c*}}{\partial \kappa^c} + \frac{\partial F^{c*}}{\partial \bar{\boldsymbol{\sigma}}^*} : \frac{\partial \left(\boldsymbol{A}^{\bar{\sigma},pc} \right)}{\partial \kappa^c} : \bar{\boldsymbol{\sigma}} \right) \frac{d\kappa^c}{d\lambda}, \tag{116}$$

$$\frac{\partial F^{c*}}{\partial \bar{\boldsymbol{\sigma}}^*} = \sqrt{\frac{3}{2}} \frac{\bar{\boldsymbol{s}}^*}{\|\bar{\boldsymbol{s}}^*\|} + \alpha \boldsymbol{I}, \tag{117}$$

$$\frac{\partial F^c}{\partial \kappa^c} = \frac{\partial F^{c*}}{\partial \kappa^c} + \frac{\partial F^{c*}}{\partial \bar{\boldsymbol{\sigma}}^*} : \frac{\partial \boldsymbol{A}^{\bar{\sigma},pc}}{\partial \kappa^c} : \bar{\boldsymbol{\sigma}}, \tag{118}$$

$$\frac{\partial F^{t*}}{\partial \kappa^t} = -(1-\alpha) E^{pc*}, \tag{119}$$

$$\left[\frac{\partial A^{\bar{\sigma},pc}}{\partial \kappa^c} \right]_{1111} = \frac{E^{pc*} \bar{f}_{11}^c - E_{11}^{pc} \bar{f}^{c*}}{\left(\bar{f}_{11}^c \right)^2}, \quad \left[\frac{\partial A^{\bar{\sigma},pc}}{\partial \kappa^c} \right]_{2222} = \frac{E^{pc*} \bar{f}_2^c - E_{22}^{pc} \bar{f}^{c*}}{\left(\bar{f}_{22}^c \right)^2},$$

$$\left[\frac{\partial A^{\bar{\sigma},pc}}{\partial \kappa^c} \right]_{1212} = \frac{(1-\alpha)\left(E^{pc*} \bar{f}_{12}^c - E_{12}^{pc} \bar{f}^{c*} \right)}{2\sqrt{3}\left(\bar{f}_{12}^c \right)^2}, \quad \left[\frac{\partial A^{\bar{\sigma},pc}}{\partial \kappa^c} \right]_{2121} = \frac{(1-\alpha)\left(E^{pc*} \bar{f}_{12}^c - E_{12}^{pc} \bar{f}^{c*} \right)}{2\sqrt{3}\left(\bar{f}_{12}^c \right)^2},$$

$$\left[\frac{\partial A^{\bar{\sigma},pc}}{\partial \kappa^c}\right]_{1221} = \frac{(1-\alpha)\left(E^{pc*}\bar{f}_{12}^c - E_{12}^{pc}\bar{f}^{c*}\right)}{2\sqrt{3}\left(\bar{f}_{12}^c\right)^2}, \quad \left[\frac{\partial A^{\bar{\sigma},pc}}{\partial \kappa^c}\right]_{2112} = \frac{(1-\alpha)\left(E^{pc*}\bar{f}_{12}^c - E_{12}^{pc}\bar{f}^{c*}\right)}{2\sqrt{3}\left(\bar{f}_{12}^c\right)^2},$$
$$\left[\frac{\partial A^{\bar{\sigma},pc}}{\partial \kappa^c}\right]_{\text{else}} = 0. \tag{120}$$

Appendix C: Computation of $\dot{d}^+$, $\dot{d}^-$, $\dot{s}$, and d^{II}

(i) Computation of $\dot{d}^+$:

$$\dot{d}^+ = \frac{\mathrm{d}G^{+*}}{\mathrm{d}\tau^{+*}}\frac{\mathrm{d}\tau^{+*}}{\mathrm{d}\bar{\boldsymbol{\sigma}}^{+*}}\frac{\mathrm{d}\bar{\boldsymbol{\sigma}}^{+*}}{\mathrm{d}\bar{\boldsymbol{\sigma}}^{+}}\frac{\mathrm{d}\bar{\boldsymbol{\sigma}}^{+}}{\mathrm{d}\bar{\boldsymbol{\sigma}}}\dot{\bar{\boldsymbol{\sigma}}} = h^{d+*}\left(\frac{\boldsymbol{M}^{t*}:\bar{\boldsymbol{\sigma}}^{+*}}{2\tau^{+*}} + \frac{1}{2}\boldsymbol{\pi}\right) : \boldsymbol{A}^{\bar{\sigma},d+} : \boldsymbol{Q}^{+} : \dot{\bar{\boldsymbol{\sigma}}} \tag{121}$$

where

$$h^{d+*} = \frac{A^+ r^{+*} + r^{0+*}}{\left(r^{+*}\right)^2} e^{A^+\left(1-\frac{r^{+*}}{r^{0+*}}\right)}, \tag{122}$$

$$\boldsymbol{Q}^{+} = \sum_i H\left(\hat{\bar{\sigma}}_i\right)\boldsymbol{P}_{ii}\otimes\boldsymbol{P}_{ii} + 2\sum_{\substack{i,j\\ j>i}}\frac{\left\langle\hat{\bar{\sigma}}_i\right\rangle - \left\langle\hat{\bar{\sigma}}_j\right\rangle}{\hat{\bar{\sigma}}_i - \hat{\bar{\sigma}}_j}\boldsymbol{P}_{ij}\otimes\boldsymbol{P}_{ij}, \tag{123}$$

$$\boldsymbol{P}_{ii} = \boldsymbol{p}_i\otimes\boldsymbol{p}_i, \quad \boldsymbol{P}_{ij} = \frac{1}{2}\left(\boldsymbol{p}_i\otimes\boldsymbol{p}_j + \boldsymbol{p}_j\otimes\boldsymbol{p}_i\right); \tag{124}$$

(ii) Computation of $\dot{d}^-$:

$$\dot{d}^- = \frac{\mathrm{d}G^{-*}}{\mathrm{d}\tau^{-*}}\frac{\mathrm{d}\tau^{-*}}{\mathrm{d}\bar{\boldsymbol{\sigma}}^{*}}\frac{\mathrm{d}\bar{\boldsymbol{\sigma}}}{\mathrm{d}\bar{\boldsymbol{\sigma}}}\dot{\bar{\boldsymbol{\sigma}}} = h^{d-*}\left(\frac{K}{\sqrt{3}}\boldsymbol{I} + \sqrt{2}\bar{\boldsymbol{s}}^{*}\right) : \boldsymbol{A}^{\bar{\sigma},d+} : \dot{\bar{\boldsymbol{\sigma}}} \tag{125}$$

where $\bar{\boldsymbol{s}}^*$ is the deviatoric stress tensor of $\bar{\boldsymbol{\sigma}}^*$, and h^{d-*} is expressed as

$$h^{d-*} = \begin{cases} \frac{a^- r^{e-*}}{\left(r^{p-*}-r^{0-*}\right)^2}\left(1 - \frac{2r^{0-*}}{\left(r^{-*}\right)^2}\right), & r^{0-*} \le r^{-*} \le r^{p-*} \\ \frac{r^{e-*}}{\left(r^{-*}\right)^2}\operatorname{sech}^2\left(1 + 2r^{-*}\tanh\frac{b^-}{r^{p-*}}\right), & r^{-*} > r^{p-*}; \end{cases} \tag{126}$$

(iii) Computation of $\dot{s}$:

$$\dot{s} = \frac{1}{2}\frac{\boldsymbol{I}\left(\sum_i\left|\hat{\bar{\sigma}}_i\right|\right) - \bar{I}_1\left(\sum_i \boldsymbol{P}_{ii}\right)}{\left(\sum_i\left|\hat{\bar{\sigma}}_i\right|\right)^2} : \dot{\bar{\boldsymbol{\sigma}}}; \tag{127}$$

(iv) Computation of $\dot{d}^{\text{II}}$:

$$\dot{d}^{\text{II}} = \frac{\mathrm{d}G^{\text{II}}}{\mathrm{d}\tau^{\text{II}}}\frac{\mathrm{d}\tau^{\text{II}}}{\mathrm{d}\bar{\boldsymbol{\sigma}}}\dot{\bar{\boldsymbol{\sigma}}} = h^{\text{II}}\boldsymbol{\xi}^{\text{II}} : \dot{\bar{\boldsymbol{\sigma}}} \tag{128}$$

where

$$h^{\text{II}} = \frac{B^{\text{II}} r^{\text{II}} + r^{0,\text{II}}}{\left(r^{\text{II}}\right)^2} e^{B^{\text{II}}\left(1-\frac{r^{\text{II}}}{r^{0,\text{II}}}\right)}, \tag{129}$$

$$\boldsymbol{\xi}^{\text{II}} = \begin{bmatrix} 0 & \frac{1}{2}\operatorname{sign}\left(\bar{\sigma}_{12}\right) \\ \frac{1}{2}\operatorname{sign}\left(\bar{\sigma}_{12}\right) & \tan\phi^{\text{II}} \end{bmatrix}. \tag{130}$$

References

1. Tomazevic, M.: Earthquake-Resistant Design of Masonry Buildings. Imperial College Press, London (1999)
2. Roca, P., Cervera, M., Gariup, G., Pela, L.: Structural analysis of masonry historical constructions. Classical and advanced approaches. Arch. Comput. Methods Eng. **17**(3), 299–325 (2010)
3. Theodossopoulos, D., Sinha, B.: A review of analytical methods in the current design processes and assessment of performance of masonry structures. Constr. Build. Mater. **41**, 990–1001 (2013)
4. Lourenço, P.B.: Computational strategies for masonry structures. Ph.D. thesis, Department of Civil Engineering, Delft University of Technology, Delft, The Netherlands (1996)
5. Lotfi, H.R., Shing, P.B.: Interface model applied to fracture of masonry structures. J. Struct. Eng. ASCE **120**(1), 63–80 (1994)
6. Tzamtzis, A.: Dynamic finite element analysis of complex discontinuous and jointed structural systems using interface elements. Ph.D. thesis, Department of Civil Engineering, Queen Mary University of London, UK (1994)
7. Gambarotta, L., Lagomarsino, S.: Damage models for the seismic response of brick masonry shear walls. Part I: the mortar joint model and its applications. Earthq. Eng. Struct. Dyn. **26**(4), 423–439 (1997)
8. Gambarotta, L., Lagomarsino, S.: Damage models for the seismic response of brick masonry shear walls. Part II: the continuum model and its applications. Earthq. Eng. Struct. Dyn. **26**(4), 441–462 (1997)
9. Lourenço, P.B., Rots, J.G.: Multisurface interface model for analysis of masonry structures. J. Eng. Mech. ASCE **123**(7), 660–668 (1997)
10. Sutcliffe, D., Yu, H., Page, A.: Lower bound limit analysis of unreinforced masonry shear walls. Comput. Struct. **79**(14), 1295–1312 (2001)
11. Cervera, M., Oliver, J., Manzoli, O.: A rate-dependent isotropic damage model for the seismic analysis of concrete dams. Earthq. Eng. Struct. Dyn. **25**(9), 987–1010 (1996)
12. Faria, R., Oliver, J., Cervera, M.: A strain-based plastic viscous-damage model for massive concrete structures. Int. J. Solids Struct. **35**(14), 1533–1558 (1998)
13. Hatzigeorgiou, G.D., Beskos, D.E.: Static analysis of 3-D damaged solids and structures by BEM. Eng. Anal. Bound. Elem. **26**(6), 521–526 (2002)
14. Hatzigeorgiou, G.D., Beskos, D.E.: Dynamic inelastic structural analysis by the BEM: a review. Eng. Anal. Bound. Elem. **35**(2), 159–169 (2011)
15. Voyiadjis, G.Z., Kattan, P.I.: Mechanics of damage processes in series and in parallel: a conceptual framework. Acta Mech. **223**, 1863–1878 (2012)
16. Baratta, A., Corbi, H., Corbi, O.: Theorems for masonry solids with brittle time-decaying tensile limit strength. Acta Mech. **228**, 837–849 (2017)
17. Lourenço, P.B., De Borst, R., Rots, J.G.: A plane stress softening plasticity model for orthotropic materials. Int. J. Numer. Methods Eng. **40**(21), 4033–4057 (1997)
18. Lourenço, P.B., Rots, J.G., Blaauwendraad, J.: Continuum model for masonry: parameter estimation and validation. J. Struct. Eng. ASCE **124**(6), 642–652 (1998)
19. Berto, L., Saetta, A., Scotta, R., Vitaliani, R.: An orthotropic damage model for masonry structures. Int. J. Numer. Methods Eng. **55**(2), 127–157 (2002)
20. Bensoussan, A., Lions, J.L., Papanicolau, G.: Asymptotic Analysis for Periodic Structures. North Holland, Amsterdam (1978)
21. Bakhvalov, N., Panasenko, G.: Homogenization: Averaging Processes in Periodic Media: Mathematical Problems in the Mechanics of Composite Materials. Kluwer Academic, Dordrecht (1989)
22. Lopez, J., Oller, S., Oñate, E., Lubliner, J.: A homogeneous constitutive model for masonry. Int. J. Numer. Methods Eng. **46**(10), 1651–1671 (1999)
23. Van der Pluijm, R.: Out-of-plane bending of masonry: behaviour and strength. Ph.D. thesis, Department of Architecture, Building and Planning, Eindhoven University of Technology, Eindhoven, The Netherlands (1999)
24. Zucchini, A., Lourenço, P.: A micro-mechanical model for the homogenisation of masonry. Int. J. Solids Struct. **39**(12), 3233–3255 (2002)
25. Ziegler, F.: Mechanics of Solids and Fluids, 2nd edn. Springer, New York (1995)
26. Sobotka, Z.: Theorie des plastischen Fließens von anisotropen Kőrpern. Zeitschrift fur Angewandte Mathematik und Mechanik (ZAMM) **49**(1–2), 25–32 (1969)
27. Boehler, J., Sawczuk, A.: Equilibre limite des sols anisotropes. J. Mécanique **9**(1), 5–33 (1970)
28. Betten, J.: Applications of tensor functions to the formulation of yield criteria for anisotropic materials. Int. J. Plast. **4**(1), 29–46 (1988)
29. Barlat, F., Lege, D.J., Brem, J.C.: A six-component yield function for anisotropic materials. Int. J. Plast. **7**(7), 693–712 (1991)
30. Karafillis, A., Boyce, M.: A general anisotropic yield criterion using bounds and a transformation weighting tensor. J. Mech. Phys. Solids **41**(12), 1859–1886 (1993)
31. Oller, S., Botello, S., Miquel, J., Oñate, E.: An anisotropic elastoplastic model based on an isotropic formulation. Eng. Comput. **12**(3), 245–262 (1995)
32. Oller, S., Car, E., Lubliner, J.: Definition of a general implicit orthotropic yield criterion. Comput. Methods Appl. Mech. Eng. **192**(7), 895–912 (2003)
33. Pelà, L., Cervera, M., Roca, P.: Continuum damage model for orthotropic materials: application to masonry. Comput. Methods Appl. Mech. Eng. **200**(9), 917–930 (2011)
34. Pelà, L., Cervera, M., Roca, P.: An orthotropic damage model for the analysis of masonry structures. Constr. Build. Mater. **41**, 957–967 (2013)
35. Barlat, F., Aretz, H., Yoon, J., Karabin, M., Brem, J., Dick, R.: Linear transformation-based anisotropic yield functions. Int. J. Plast. **21**(5), 1009–1039 (2005)
36. Barlat, F., Lian, K.: Plastic behavior and stretchability of sheet metals. Part I: a yield function for orthotropic sheets under plane stress conditions. Int. J. Plast. **5**(1), 51–66 (1989)

37. Simo, J.C., Hughes, T.J.R.: Computational Inelasticity. Springer, New York (1998)
38. Lemaitre, J., Chaboche, J.: Mechanics of Solid Materials. Cambridge University Press, Cambridge (1994)
39. Simo, J., Ju, J.: Strain-and stress-based continuum damage models—I. Formulation. Int. J. Solids Struct. **23**(7), 821–840 (1987)
40. Faria, R., Oliver, J., Cervera, M.: Modeling material failure in concrete structures under cyclic actions. J. Struct. Eng. ASCE **130**(12), 1997–2005 (2004)
41. Lee, J., Fenves, G.L.: Plastic-damage model for cyclic loading of concrete structures. J. Eng. Mech. ASCE **124**(8), 892–900 (1998)
42. Drucker, D.C., Prager, W.: Soil mechanics and plastic analysis or limit design. Q. Appl. Math. **10**(2), 157–165 (1952)
43. Mazars, J.: A description of micro- and macroscale damage of concrete structures. Eng. Fract. Mech. **25**(5), 729–737 (1986)
44. Mazars, J., Pijaudier-Cabot, G.: Continuum damage theory application to concrete. J. Eng. Mech. ASCE **115**(2), 345–365 (1989)
45. Oliver, J., Cervera, M., Oller, S., Lubliner, J.: Isotropic damage models and smeared crack analysis of concrete. In: Proceedings of SCI-C Computer Aided Analysis and Design of Concrete Structures, pp. 987–1010. Pineridge Press, Swansea (1990)
46. ANSYS Engineering Simulation Software: User's Manual, Version 13. ANSYS Inc., Canonburg (2010)
47. Nazar, M.E., Sinha, S.N.: Loading–unloading curves of interlocking grouted stabilised sand–flyash brick masonry. Mater. Struct. **40**(7), 667–678 (2007)
48. Nazar, M.E., Sinha, S.N.: Behavior of interlocking grouted stabilized sand–fly ash brick masonry under uniaxial cyclic compressive loading. J. Mater. Civ. Eng. **19**(11), 947–956 (2007)
49. Raijmakers, T.M.J., Vermeltfoort, A.T.: Deformation controlled meso shear tests on masonry piers. In: Report B-92-1156, TNO-BOUW, Building and Construction Research, Eindhoven University of Technology, The Netherlands (1992)